https://doi.org/10.5194/egusphere-2025-649
Preprint. Discussion started: 12 March 2025

The impacts of secondary ice production on the microphysics and dynamics of mid-latitude cold season convection

Zhipeng Qu[1], Alexei Korolev[1], Jason A. Milbrandt[1], Ivan Heckman[1], Mélissa Cholette[1], Cuong Nguyen[2], Mengistu Wolde[2]

[1]Meteorological Research Division, Environment and Climate Change Canada, Toronto, Ontario, Canada
[2]National Research Council Canada, Ottawa, Canada

Correspondence to: Zhipeng Qu (zhipeng.qu@ec.gc.ca)

Abstract. This study examines the impact of inclusion of secondary ice production (SIP) parameterizations on the cloud microphysics and dynamics in numerical weather prediction (NWP) simulations under mid-latitude winter conditions. Hindcast mesoscale model simulations were performed for two flights from the 2019 In-Cloud ICing and Large-drop Experiment (ICICLE) field campaign. The simulations used a horizontal grid spacing of 250 meters and employed a detailed triple-moment bulk microphysics scheme capable of predicting the liquid fraction of hydrometeors. SIP processes, including the Hallett-Mossop (HM) and fragmentation of freezing drops (FFD), are parameterized in this study. The NWP simulation results are compared with observational data collected during the ICICLE campaign. Sensitivity tests were conducted to highlight the importance of better quantifying SIP production rate in the NWP models. The findings indicate that SIP significantly enhances the simulated cloud ice number concentration and ice water content, particularly under strong convective conditions during winter. Additionally, the results reveal that the simulations are highly sensitive to the parameterization of HM and FFD processes due to the interaction between these two SIP mechanisms. High ice water content (HIWC) production is closely associated with SIP in strong convective conditions, whereas in stratiform conditions, HIWC can occur without a significant impact from SIP.

1 Introduction

Secondary ice production (SIP) is recognized as a fundamental process in cloud microphysics (e.g., Cantrell and Heymsfield, 2005; Field et al., 2017). SIP primarily enhances ice particle concentrations, often exceeding those from primary ice production (PIP) by several orders of magnitude (e.g., Hobbs and Rangno, 1985; Ladino et al., 2017). This significant increase in ice particle concentration can profoundly impact the phase composition, cloud dynamics, precipitation rates, and cloud radiative properties, thereby influencing the energy balance and hydrological cycle on both regional and global scales. At present, seven mechanisms are recognized as sources of secondary ice in clouds. These include the fragmentation of freezing droplets (FFD) (e.g., Kleinheins et al., 2021), rime splintering (the Hallett-Mossop process, HM) (e.g., Hallett and Mossop, 1974), fragmentation due to ice-ice collisions (e.g., Vardiman, 1978; Takahashi et al., 1995), ice fragmentation due to thermal shock (e.g., Dye and Hobbs, 1968), fragmentation of sublimating ice (Oraltay and Hallett, 1989), activation of ice-nucleating particles

https://doi.org/10.5194/egusphere-2025-649
Preprint. Discussion started: 12 March 2025

(INPs) in transient supersaturation around freezing drops (e.g., Prabhakaran et al., 2020), and the break-up of freezing water drops upon impact with ice particles (James et al., 2021). The first six mechanisms are reviewed and summarized by Korolev and Leisner (2020). Among these, HM and FFD are the most experimentally studied SIP mechanisms. However, detailed analyses of previous experiments by Korolev and Leisner (2020) revealed a large variability in ice production rates, indicating that these SIP processes require further study. The other four mechanisms have been explored in a limited number of laboratory experiments, addressing only a subset of environmental conditions (e.g., fragmentation during ice collisions, fragmentation of sublimating ice) or merely demonstrating the general feasibility of SIP mechanisms (e.g., fragmentation due to thermal shock, activation of INPs in transient supersaturation around freezing drops). Consequently, Korolev and Leisner (2020) concluded that the relative contributions of each of the six SIP mechanisms to the enhancement of ice concentrations remain uncertain.

In recent years, many studies have investigated the effect of SIP on cloud microphysics with the help of model simulations (e.g., Phillips et al., 2017, 2018; Sullivan et al., 2018; Hoarau et al., 2018; Fu et al., 2019; Sotiropoulou et al., 2020, 2021; Dedekind et al., 2021; Hawker et al., 2021; Huang et al., 2021, 2022). Most of these modeling efforts were focused on matching simulated moments of particle size distributions (PSDs) with those observed *in situ*. In many ways, the implementation of SIP in numerical models was hindered by the lack of consensus on parameterizations of SIP mechanisms.

Previous studies have also shown that the occurrence of high ice water content (HIWC) is linked to an increase in ice particle concentrations driven by SIP processes. HIWC conditions are defined as cloud environments with ice water content (IWC) exceeding 1 g m^{-3}. These conditions present significant hazards for civil aviation, potentially leading to engine power loss, stalls, or structural damage (e.g., Lawson et al. 1998; Mason et al. 2006, Mason and Grzych, 2011). The phenomenon of HIWC is well documented from *in situ* observations in tropical mesoscale convective systems (MCSs) (e.g., Heymsfield and Palmer 1986, Lawson et al., 1998, Gayet et al., 2012, Fridlind et al., 2015; Leroy et al., 2017, Strapp et al., 2021). Several previous modeling studies using different cloud microphysical parameterizations attempted to reproduce high IWCs. Ackerman et al. (2015) used a 1D model to explore microphysics in tropical MCSs. Simulations performed with 3D models (Franklin et al., 2016; Stanford et al., 2017; Qu et al., 2018) pointed to the inaccuracies in the estimation of cloud PSD, IWC, and ice category comparing to the observations. Huang et al. (2021) conducted high-resolution simulations of tropical convection and found significant overestimates of radar reflectivity (Z) and underestimates of total ice crystal concentration (Ni). Adding SIP in high-resolution simulations with advanced microphysical scheme, Huang et al. (2022) found significant improvement of the simulated Ni matching to the *in situ* observations. Similarly, Qu et al. (2022) conducted idealized simulation for tropical convection and found that SIP significantly enhances the IWC and Ni, and reduces the simulated Z. The size of anvil cloud also increased when SIP is included in the simulation. Korolev et al. (2024), based on *in situ* observations and idealized high-resolution simulations, demonstrated that SIP in the vicinity of the melting layer plays a crucial role in the formation, maintenance, and longevity of HIWC in tropical MCSs. Recirculation of droplets through the melting layer by convective updrafts was identified as a primary mechanism providing a high concentration of large, supercooled drops, which initiated a massive production of secondary ice due to the SIP FFD process.

https://doi.org/10.5194/egusphere-2025-649
Preprint. Discussion started: 12 March 2025

Although most HIWC conditions occur in tropical regions, they can also be encountered in mid-latitude regions, even during winter, as HIWC-related aircraft issues have been reported. Rugg et al. (2022) examine these conditions using ICICLE observations and raise questions about the possible role of SIP in contributing to the formation of HIWC conditions. In addition to influencing HIWC conditions, SIP could also impact other cloud microphysical processes during winter. Cholette et al. (2024) assessed the impact of incorporating the HM process in 2.5 km resolution NWP simulations, demonstrating significant improvements in freezing rain forecasts. Similarly, Lachapelle et al. (2024) examined the influence of SIP on ice pellet simulations and reported enhanced predictive performance.

The first objective of this study is to examine the impact of inclusion of SIP in the simulation of mid-latitude winter convection, with a particular focus on the link between SIP and HIWC condition and how this compares to the impacts previously observed in tropical convection. Since different parameterization approaches for various SIP mechanisms can impact model simulation results, the second objective is to explore the sensitivity of parameterized mechanisms of HM and FFD for mid-latitude winter conditions. This sensitivity study underscores the importance of better quantifying SIP production rates in nature under different atmospheric conditions.

The remainder of the paper is structured as follows. The next section describes the observational data used for evaluation. Section 3 details the model configuration, the microphysics scheme, and the parameterizations of SIP. Section 4 describes the various experiments conducted in this study. Section 5 evaluates the simulation results for two ICICLE flights. The differences of ice particle size distribution between mid-latitude winter convection and tropical convection are discussed in Section 6. The final section presents the conclusions and perspectives of the study.

2. Observation data

In situ data used in this study were collected from the National Research Council Canada (NRC) Convair-580 research aircrafts. The flight operations of the NRC Convair-580 in the frame of the ICICLE campaign were performed in the Great Lakes region of the United States from January to March 2019 (DiVito et al. 2020; Bernstein et al. 2021a, b). The ICICLE campaign focused on improving the understanding of aircraft icing hazards, specifically those caused by in-cloud supercooled large droplets (SLD).

The measurements of PSDs used in this study were performed by three particle probes, which covered different particle size ranges. The Droplet Measurement Technologies (DMT) Cloud Droplet Probe (CDP: Lance et al., 2010) was used for measurements of droplets in size range 2 μm < D < 50 μm. The Stratton Park Engineering Company (SPEC) 2D imaging-stereo (2D-S: Lawson et al. 2006) covered the nominal size range from 10 to 1250 μm. The DMT Precipitation Imaging Probe (PIP: Baumgardner et al., 2001) provided measurements of particles in the nominal size range from 100 μm to 6.4 mm (PSD). The processing software employed a retrieval algorithm of partially viewed particle images (Heymsfield and Parrish, 1979;

Korolev and Sussman, 2000), which allowed the enhancement of particle statistics and extended the maximum size of the composite PSD up to 12.8 mm.

All particle probes were equipped with anti-shattering tips to mitigate the effect of ice shattering on the measurements of ice particle concentration (Korolev et al., 2013). Residual shattering artifacts were identified and filtered out with the help of the inter-arrival time algorithm (Field et al., 2006; Korolev and Fields 2015). Cloud particle number concentration, characteristic sizes of ice and liquid particles, ice and liquid water content (LWC) were calculated from PSDs measured by particle probes.

During the ICICLE project, the NRC Convair-580 was also equipped with the NRC Airborne W and X-bands (NAWX) radar system (Wolde & Pazmany, 2005). The radar reflectivity from the X-band of the NAWX radar is used to characterize the cloud macrophysical structure and asses the result of the SIP simulations.

3. Model simulation

3.1. Model configuration

The numerical model used in this study is the Global Environmental Multiscale (GEM) model (Côté et al., 1998; Girard et al., 2014). GEM is used for operational numerical weather prediction (NWP) in Environment and Climate Change Canada (ECCC) as well as research in ECCC and Canadian universities. The dynamical core of GEM is formulated based on the non-hydrostatic fully compressible primitive equations with a terrain-following hybrid vertical grid. As such, it can be run at cloud-resolving (sub-km grid spacing) scales. It can be run on global or limited-area domains and is capable of one-way nesting. In this study, four cascade domains with horizontal grid-spacings of 10, 2.5, 1.0 and 0.25 km and sizes of 3600×2600 km^2, 1800×1800 km^2, 1024×1024 km^2 and 512×512 km^2 are used respectively. The high-resolution simulation with a grid spacing of 0.25 km provides enhanced capability to resolve small-scale phenomena such as convective updrafts and the recirculation of raindrops by these updrafts near the melting layer. Accurately resolving these physical processes is crucial for better representing SIP mechanisms, including both HM and FFD process (Korolev et al., 2024). For ICICLE Flight 9, the simulation is initiated at 12:00 UTC on 2019-02-07 and runs for 12 hours. All four nesting domains are centred on 44.5ºN and 88.75ºW (Figure 1). For ICICLE Flight 20, the simulation is initiated at 06:00 UTC on 2019-02-23 and runs for 12 hours, with all four nesting domains centred on 42.7°N and 89.9°W (Figure 1). 84 unevenly spaced hybrid vertical levels are used for 10 km simulations and 62 levels are used for all other simulations.

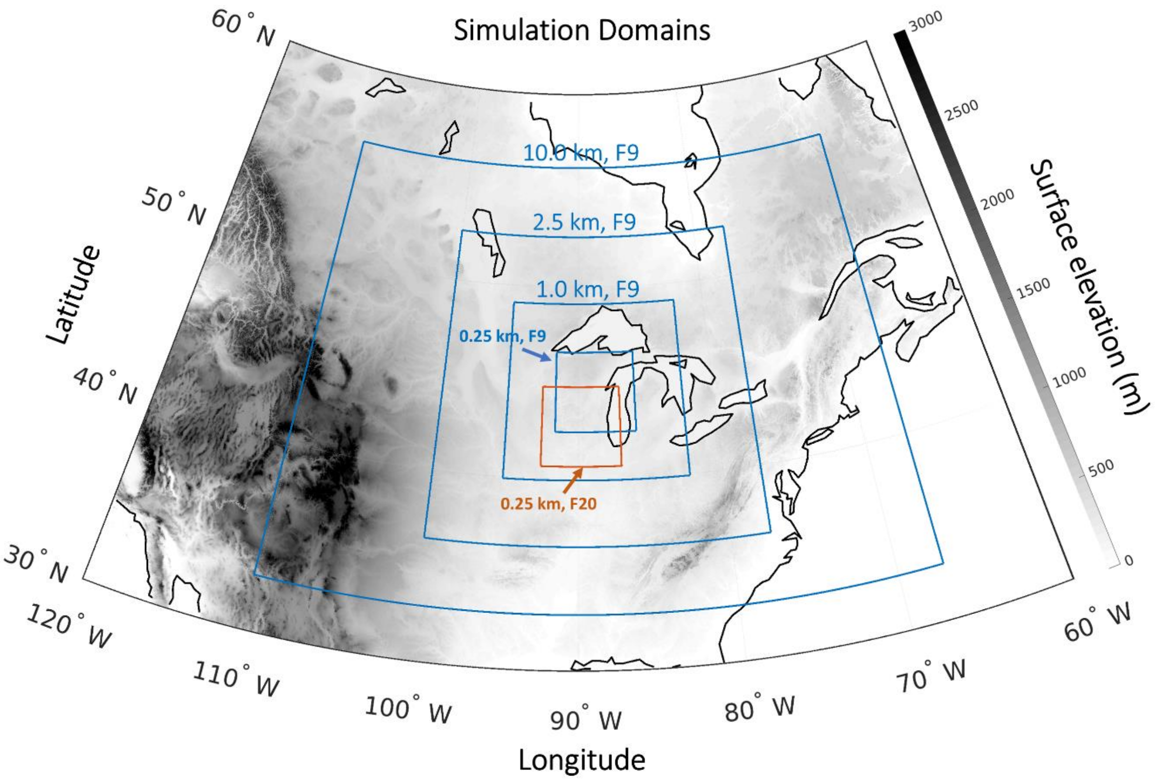

Figure 1. Simulation domains at different stages of the cascade for ICICLE Flight 09 (blue rectangles), ranging from 10 km to 0.25 km resolution. The red rectangle marks the innermost 0.25 km domain for Flight 20. The three outer domains for Flight 20 follow a similar pattern to Flight 09 but are shifted, as they center on the red rectangle. The grayscale shading represents surface elevation in meters, while black lines indicate waterfront contours.

3.2. Cloud microphysics scheme

In the GEM simulations of this study, all grid-scale cloud microphysical processes were represented by the Predicted Particle Properties (P3) bulk microphysics scheme, originally described in Morrison and Milbrandt (2015). P3 has a unique way of representing ice-phase hydrometeors using a generic ice-phase category with freely evolving bulk physical properties. Since its inception there have been several major modifications to the P3 scheme including the generalization to a user-specified number of generic ice categories (Milbrandt and Morrison, 2016), a triple-moment treatment of ice (Milbrandt et al., 2021; Morrison et al. 2004), and a prognostic liquid fraction for wet ice (Cholette et al., 2019, 2024). In this study, four ice categories were used in all high-resolution simulations. The particle size distribution (PSD) of each ice category is represented by a complete gamma function and each category has six prognostic (i.e., advected) mixing ratio variables: total ice mass, rime mass, liquid ice mass, bulk rime volume, total ice number, ice reflectivity factor. These prognostic variable fields enable the computation of various bulk physical properties (e.g. density, rime fraction, etc.) which vary continuously in time and space.

The decision to use four ice categories was made to maximize the representation of the multi-modal ice particle size distribution during conditions of high SIP rate where large pre-existing ice particles coexist with small ice splinters. Qu et al. (2022) showed that three ice categories in the P3 scheme are sufficient to effectively capture the size distribution when SIP is active; Milbrandt et al. (2024) showed a similar "convergence" with three categories for the simulation of hail. Nevertheless, four categories were used in this study since the additional category should, in principle, model the total ice phase slightly better without significantly increasing computational cost.

3.3. Parameterization of SIP

This study focuses on assessing the impact of including two SIP processes in the NWP simulations: the HM rime splintering process and the FFD process. As discussed, additional SIP processes are currently known; however, due to limited understanding of each, including HM and FFD, this study examines only these relatively better-characterized processes. Future studies will aim to incorporate more SIP processes.

3.3.1 Rime splintering/Hallet-Mossop (HM)

The parameterized HM process follows Hallet and Mossop (1974) stating the production of a peak value of 350 ice splinter per mg of collected liquid water during riming of liquid cloud drops or rains droplets within a temperature range of -3°C > T > -8°C, with the peak value at -5°C and varying linearly to 0 at -3 and -5 °C. The size of ice splinters is set to 10 µm. This study utilizes three distinct methods to calculate the number of ice splinters produced by the HM process. In the first method (referred to as HMr), the number of ice splinters is determined based on the mass of all collected supercooled raindrops, excluding the fraction involved in the FFD process (section 3.3.2). The second method (referred to as HMgr) calculates the splinters using the mass of raindrops collected by graupel, while the third method (referred to as HMgc) uses the mass of liquid cloud droplets collected by graupel. In the P3 scheme, ice is represented as generic categories, so there is no predefined graupel category; therefore graupel is identified as ice (in a given category) with a rime fraction greater than 0.4, a bulk ice density between 50 and 700 kg m^{-3}, and a mean-mass diameter greater than 2 mm. Liquid "cloud droplets" are defined as having a diameter smaller than 50 µm, while "rain drops" have a diameter exceeding this threshold.

3.3.2 Fragmentation of Freezing Drops (FFD) process

The FFD process is parametrized following Lawson et al. (2015):

$$N_f = 2.5 \times 10^{-11} D^4, \tag{3}$$

where N_f is the average number of ice fragments per drop, and D is the freezing liquid drop diameter in micrometers. The parameterization of the FFD process was applied for raindrops (100 µm < D < 3500 µm) which were nucleated by contacting with ice particles with diameter D_i < 100 µm. Following Keinert et al. (2020) the activity of the FFD process was limited to the temperature range -25°C < T < -2°C with a maximal rate of N_f at T = -12.5ºC. The FFD rate decreases linearly from T = -12.5ºC to T = -25ºC and T = -2ºC. All newly produced ice splinters have a diameter of 10 µm.

A minimum ice mixing ratio threshold of 5×10^{-5} kg kg^{-1} was applied to activate the FFD process. The choice of this threshold was determined subjectively by trial-and-error. Its application prevents the unintended initiation of a high FFD production rate under freezing rain conditions due to the presence of very small amounts of ice. In freezing rain conditions, where large amounts of supercooled liquid raindrops are present, even a small amount of ice could trigger a chain reaction, leading to an unrealistically high ice number concentration.

In the FFD parameterization used here, supercooled rain collected by ice will freeze while producing ice splinters. Excluding the mass of ice splinters, which typically represents a small fraction of the rain mass, the remaining rain mass is added to the ice category that collected the rain. Under extreme conditions, such as when a small number of large raindrops mix with a large number of tiny ice particles, the collected rain mass added to the category of ice with very small mean-mass diameter which collect rain droplets can result in the production of a large number of mid-sized ice particles. In reality, this scenario would produce a few large ice particles and many small ones. To mitigate this effect, and following the methodology proposed by Lachapelle et al. (2024), we redirect the mass of collected rain with large mean mass-weighted diameter to the ice category that is most similar in size. This redirection takes place when the mean mass-weighted diameter of the rain is more than twice that of the ice that collect them.

In conditions with large raindrops, the FFD parameterization used in this study may produce an excessively high number of ice splinters. To limit these unrealistically large values of ice number mixing ratios, a maximum total threshold of 5×10^{7} kg^{-1} (summed across all four ice categories) is therefore applied in all simulations.

4. Establishment of experiments

An objective of this study is to examine the impacts of different approaches to modeling the HM process and its interactions with the FFD mechanism. The baseline simulation (referred to as “BASE”) is conducted with all SIP processes deactivated. Five additional simulations are performed for each case: one with only HMr (based on ice collected rain drops, excluding collected rain used for FFD), one with only FFD, and three with both HM and FFD. In the latter three, the same FFD parameterization is used, coupled with three different HM parameterizations as described in Section 3.3.1. A complete summary of all configurations is provided in Table 1. The 0.25 km simulations are designated as “[case]-[configuration],” where the case refers to either “F9” or “F20,” representing ICICLE Flight 9 or Flight 20, respectively. The configurations correspond to the names listed in the left column of Table 1. For instance, 'F9-BASE' refers to the 0.25 km baseline simulation for ICICLE Flight 9.

Table 1. List of simulations.

Experiment name	HM	FFD
BASE	off	off
HMr-FFD	HM (based on ice collected rain drops, excluding collected rain used for FFD), temperature dependent	Temperature & liquid drop size dependent
HMgr-FFD	HM (based on graupel collected rain drops), temperature dependent	
HMgc-FFD	HM (based on graupel collected liquid droplets), temperature dependent	

5. Results

This section begins by presenting the results of ICICLE Flight 9, characterized by localised convections with peak updraft speed exceeding 5 m s⁻¹. It then examines ICICLE Flight 20, which exemplifies a stratiform mesoscale system, with vertical wind velocities below 5 m s⁻¹.

5.1. ICICLE Flight 09: localized convective case

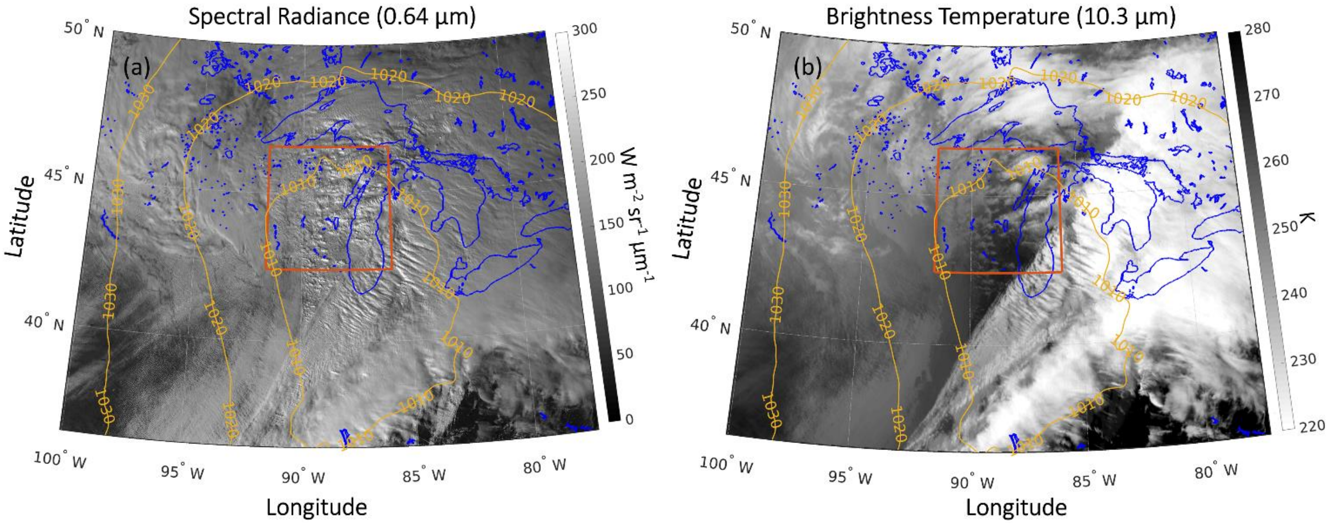

Figure 2. (a) GOES-16 spectral radiance at 0.64 µm (Channel 2). (b) GOES-16 brightness temperature at 10.3 µm (Channel 13). Both images are from 20:30 UTC on 9 February 2019. Blue lines denote coastlines and lakes; the red rectangle indicates the inner-most simulation domain (with a 0.25 km grid spacing) for Flight 9; yellow lines show the sea level pressure isobar at 18:00 UTC from the operational regional analysis used at ECCC.

On 9 February 2019, the Great Lakes region experienced a significant winter storm fuelled by a low-pressure system that intensified as it stalled over Lake Huron (Figures 2a and 2b). This system resulted in prolonged snowfall across the region. In the area west of Lake Michigan, including Wisconsin and northern Illinois, cold temperatures and snowy conditions prevailed due to the influence of a passing low-pressure system. A comparison between the visible radiances (Figure 2a) and infrared brightness temperatures (Figure 2b) from GOES-16 satellite imagery reveals scattered convective cells. These isolated convective updrafts, though sparse, were capable of producing brief bursts of snow or freezing rain.

Figure 3 shows the combined zenith and nadir pointing X-band radar reflectivity along with *in situ* observations of IWC, ice number concentration (N_i), LWC, air temperature (T), and the aircraft's altitude (H). The bright band at approximately 2.5 km is clearly visible before 20:00 UTC, but it disappears after 20:30 UTC. A temperature inversion is present near an altitude of 2 km, although the maximum temperature at this altitude remains below freezing after 20:00 UTC. Based on *in situ* observations there are many regions of mixed-phase clouds, particularly between 19:50 and 20:40 UTC and around 21:00 UTC, which provide potential favourable conditions for SIP.

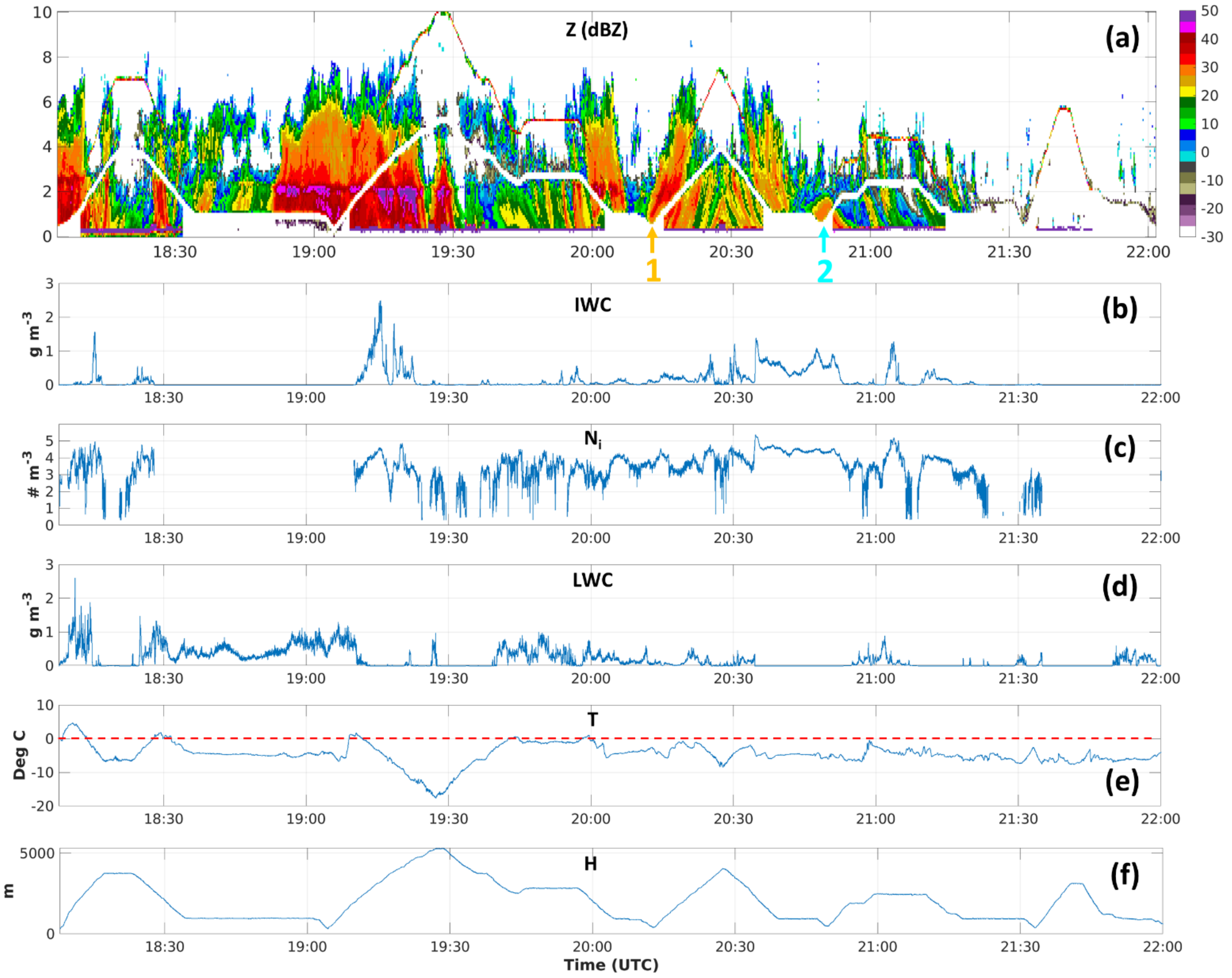

Figure 3. Data of ICICLE Flight 9 on 2019-02-07. (a): upward and downward X-band radar reflectivity (Z), (b): IWC, (c): N_i, (d): LWC, (e): T, with red dashed line indicating T=0°C, (f) H. The yellow and turquois arrows point to the two moments when Convair-580 flew a low altitude below 1 km during missed approach.

Figure 4 displays the simulated brightness temperature at 10.3 µm for the 2.5 km resolution domain (northern border limited at 50° N due to GOES-16 data availability) using the RTTOV (Radiative Transfer for TOVS) fast radiative transfer model (Saunders et al., 2018) for the F9-BASE simulation (Figure 4a). This is compared with the GOES-16 observation at 20:30 UTC on 9 February 2019 (Figure 4b). The F9-BASE simulation effectively reproduces the large-scale sea-level pressure pattern (shown by yellow lines). The simulated brightness temperature at 10.3 µm closely matches the GOES-16 observations, although it slightly underestimates cloud coverage in the southern part of Lake Michigan and the southeastern corner of the simulation domain.

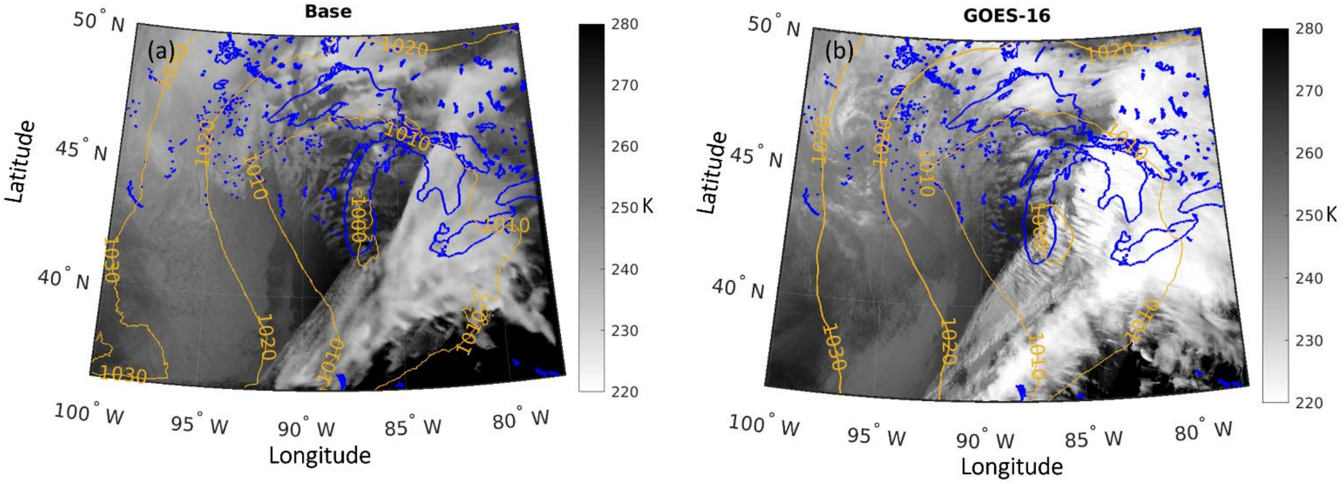

Figure 4. (a) Brightness temperature at 10.3 µm simulated using RTTOV (Saunders et al., 2018) with the BASE simulation at 2.5 km resolution for 20:30 UTC on 9 February 2019. (b) Observed brightness temperature from GOES-16 for 20:30 UTC on 9 February 2019. Blue lines indicate lake boundaries, while yellow lines represent sea-level isobars: from the F9-BASE simulation at 20:30 UTC in panel (a) and from ECCC's regional prediction model at 20:30 UTC initiated at 18:00 UTC in panel (b).

Figures 5 and 6 present the simulation profiles for the region within 10 km on each side of the aircraft track. The profiles display averaged values, except for Figure 5c, which shows 99 percentile of ice water content, the maximum vertical wind speeds (Figure 5d), and the median radar reflectivity (Z_{median}, Figure 6c). Significant variations in mean IWC among different simulations can be seen in Figure 5a. The F9-BASE simulation for ICICLE Flight 9 yields the lowest IWC, followed by slightly higher values in the F9-HMgr-FFD, while the F9-HMgc-FFD shows a notable increase. The F9-HMr-FFD simulation exhibits extremely high IWC near the surface. All SIP simulations produced a significant enhancement in the 99th percentiles of IWC at various altitudes compared to the F9-BASE simulation. The enhancement in IWC compared to the F9-BASE simulation corresponds to the increase in ice crystal number concentration (N_i) depicted in Figure 5c. The extremely high IWC observed below 1.8 km in the F9-HMr-FFD simulation (below the temperature inversion at ~2 km altitude, as shown in Figure 5e) aligns with the elevated N_i in the same altitude range (purple dash-dotted lines in Figure 5c). This IWC enhancement is strongly associated with increased freezing efficiency of liquid water (LWC and rain water content - RWC), as shown in Figure 6a and 6b, and enhanced vapor deposition growth due to the higher N_i, leading to a larger ice surface area for deposition. These findings suggest that SIP processes, such as HM and FFD, may contribute to the formation and persistence of HIWC condition.

For Z_{median} (Figure 6c), the F9-BASE and F9-HMgr-FFD simulations produce the highest values, despite having the lowest IWC. Due to the relatively low N_i in these simulations, the ice particles in F9-BASE and F9-HMgr-FFD are larger compared to those in the other two SIP simulations. F9-HMgc-FFD generates the lowest Z_{median} across most altitudes below 5 km, while F9-HMr-FFD shows even lower Z_{median} below approximately 0.9 km. This reduction in Z_{median} is due to the extremely high N_i

in F9-HMr-FFD, which significantly reduces the size of the ice particles. By 20:30 UTC, the clouds near the flight track had already glaciated, so no bright band could be seen in Figure 6c.

Although all three SIP simulations use the same FFD parameterization, differences in how the HM process is modeled result in markedly different outcomes. Figures 6d and 6e illustrate the HM and FFD rates at the simulation time step of 20:30 UTC. At this time, there is no SIP activity within 10 km of the flight track for F9-HMgr-FFD. Similar to F9-HMgr-FFD, F9-HMr-FFD calculates the number of ice splinters based on collected rain mass, but without the requirement that the ice must be graupel. By omitting this graupel condition, F9-HMr-FFD produces a high HM rate (Figure 6d, purple dash-dotted line), which subsequently triggers the FFD process, leading to an even higher FFD rate near 1 km altitude. On the other hand, F9-HMgc-FFD generates a lower HM rate near both 3.5 km and 1 km altitudes (Figure 6d, red lines). Consequently, the FFD rate is also very low near 3.8 km, with no FFD activity below 2 km. These results indicate that under freezing conditions with an abundant supply of supercooled rain, the initiation of the FFD process is highly dependent on the rate of the HM process, or potentially any SIP processes which could provide sufficient amount of small ice particles.

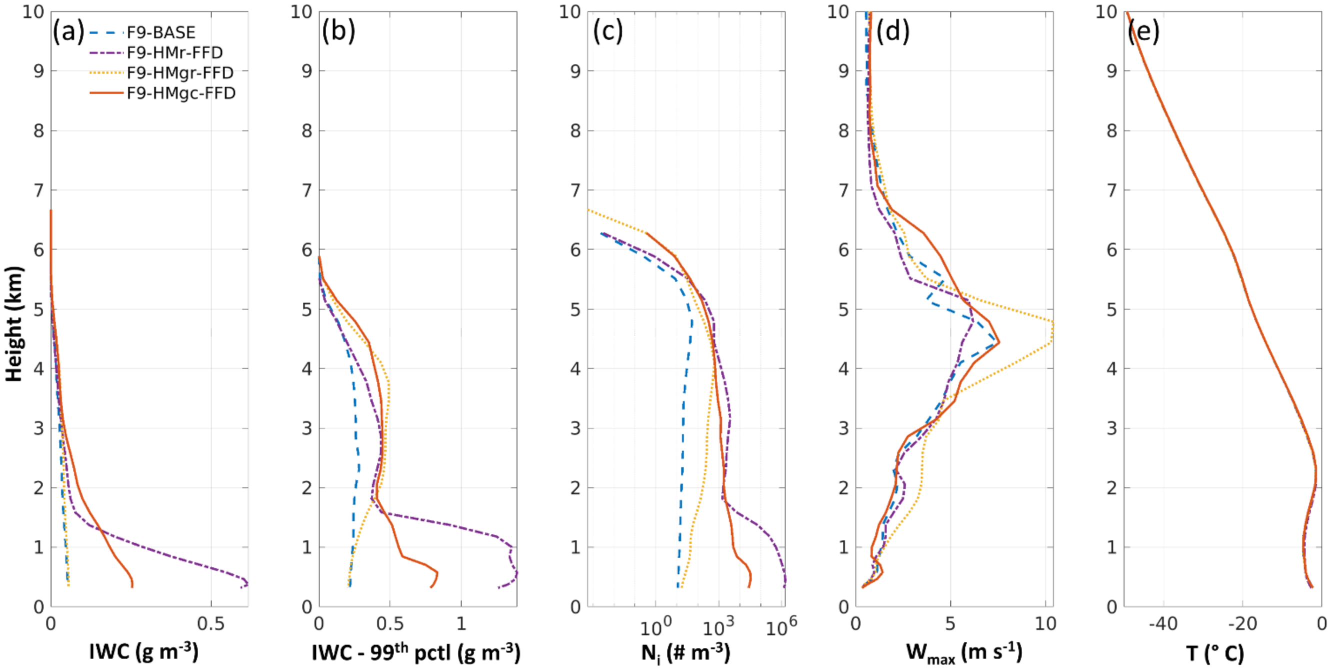

Figure 5. Profiles from the baseline and SIP simulations on 2019-02-07 for the case of ICICLE Flight 9. (a): mean IWC, (b): 95 percentile of IWC (99th pctl of IWC), (c): mean N_i with the number of ice particle smaller than 40 µm excluded, (d): maximum vertical wind speed (w_{max}), (d) T (the three simulations have only slightly different temperature that is not distinguishable in the figure). The profiles are calculated based at simulation 510 min simulation time (20:30 UTC). All profiles are calculated for the region within 10 km of distance to the aircraft track.

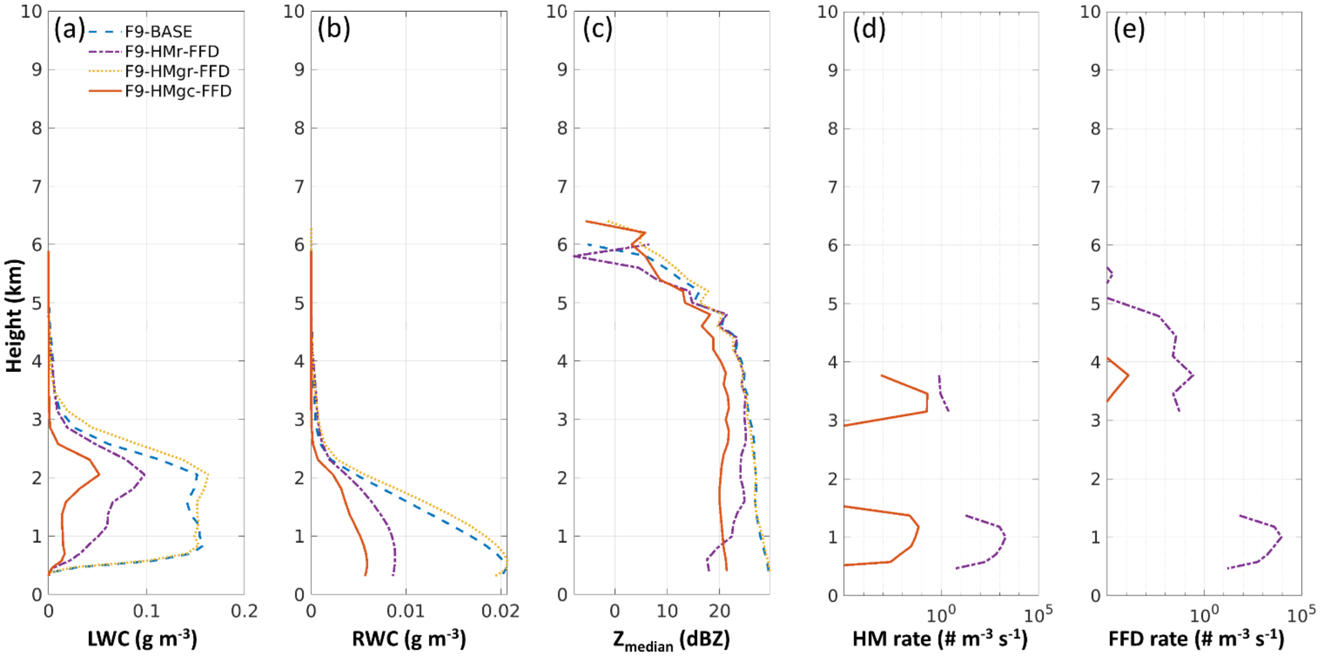

Figure 6. Profiles from the baseline and SIP simulations on 2019-02-07. (a): mean LWC, (b): mean RWC, (c): median radar reflectivity (Z_{median}), (d): mean Hallett-Mossop rate, (e): mean Fragmentation of Freezing Drop rate. All profiles are calculated for the region within 10 km of distance to the aircraft track.

To further assess the simulation results, *in situ* aircraft data were used for comparisons. Figure 7 compares the distributions of simulated IWC and N_i within 10 km of the flight track and within the flight altitude range of 0.5 to 3.8 km, with the observations shown by black lines. In the simulation results presented here, quantities from all four ice categories are summed and for the simulated N_i, ice particles smaller than 40 µm are excluded.

For IWC, the F9-BASE simulation significantly underestimates the frequency of clouds with IWC > 0.1 g m^{-3}. The F9-HMgr-FFD simulation (yellow dotted line) shows some improvement, especially for IWC > 0.5 g m^{-3}, though most frequencies remain underestimated. While F9-HMgr-FFD considerably improves the estimated IWC frequency, it still underestimates conditions of high IWC. Conversely, F9-HMr-FFD overestimates the frequency of high IWC above 0.8 g m^{-3}.

For N_i, both the F9-BASE and F9-HMgr-FFD simulations produce very low values, while HMr-FFD significantly overestimates N_i. The F9-HMgc-FFD simulation (red line) provides the closest estimate of N_i, although the peak value remains slightly lower than observed. This comparison indicates that although both F9-HMr-FFD and F9-HMgc-FFD enhance IWC and N_i, F9-HMr-FFD likely overestimates N_i significantly, and the pronounced increase in both IWC and N_i near the surface in F9-HMr-FFD, as shown in Figure 5a, 5b and 5c, is likely unrealistic. Based on this, the subsequent discussion on SIP simulations focuses exclusively on F9-HMgc-FFD.

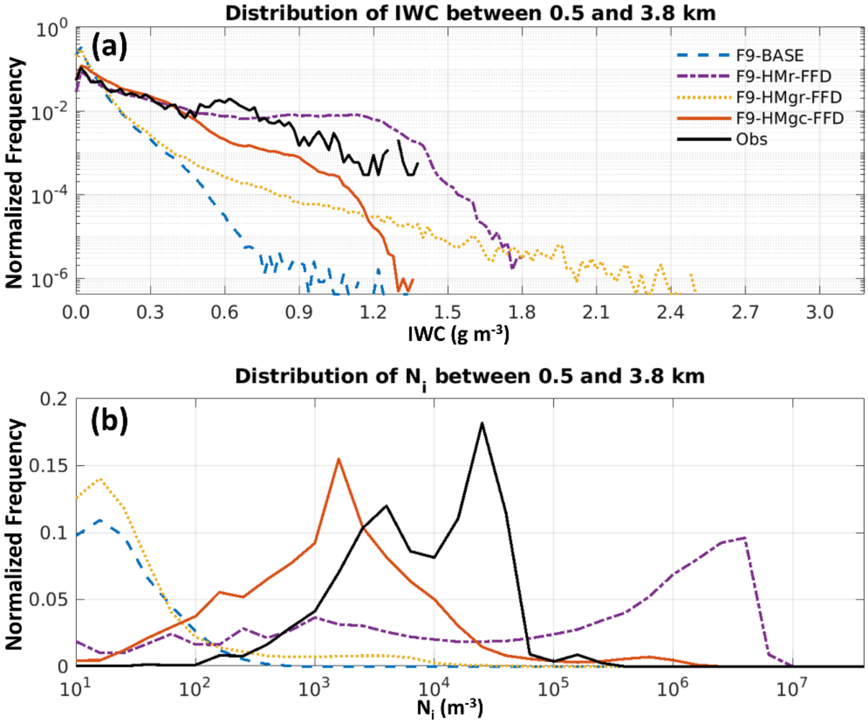

Figure 7. Distribution of IWC (a) and N_i with the number of ice particle smaller than 40 µm excluded (b) for model simulations at 20:30 UTC on 2019-02-07 and for the observation data for ICICLE Flight 9 between 18:00 and 21:00 UTC. The results from model simulations are calculated for altitudes between 0.5 and 5.5 km and with ice water content higher than 0.001 g m^{-3} in the region within 20 km of distance to the aircraft track. The results from *in situ* observation are calculated for the condition with IWC higher than 0.001 g m^{-3}. (b): logarithmic bin width of 1/5 of an order of magnitude is used. Blue dashed lines: Baseline simulation, yellow dotted lines: SIP (F9-HMr-FFD) simulation, red lines: SIP (F9-HMc-FFD) simulation, black lines: observation. 290

Comparing the simulated and observed Z values shows that the F9-HMgc-FFD simulation resulted in a closer match to the observation data (Figure 8). The F9-BASE simulation produces Z_{median} values 5 to 10 dBZ higher than observed below 5 km. 295 In contrast, F9-HMgc-FFD shows slight underestimations below 2.5 km and small overestimations between 2.5 and 5 km. There may be artifacts related to ground clutters which cause enhanced Z at altitudes twice the aircraft height, as indicated in Figure 3a. The values of Z_{median} shown in Figure 8d suggest that the simulations might underestimate above 5 km. This underestimation will be further discussed in section 5.2.

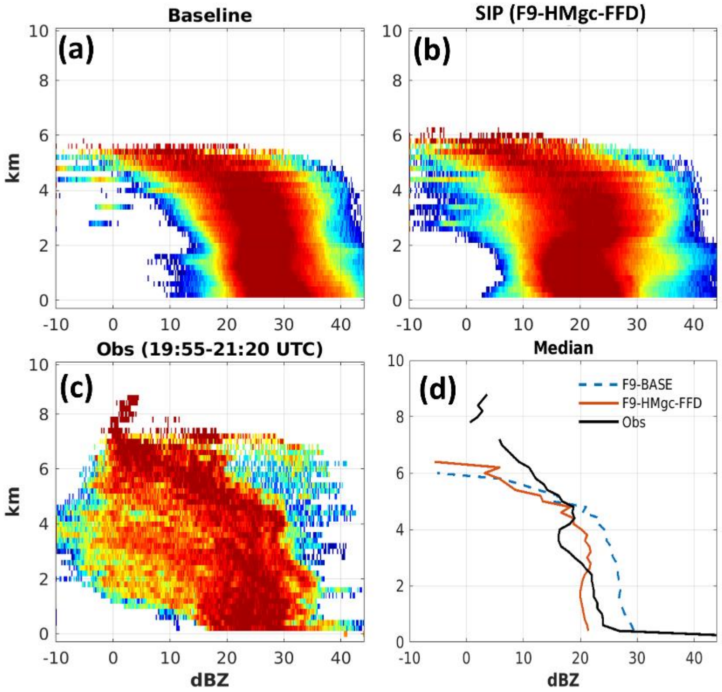

Figure 8. Z distribution frequency for (a): Baseline simulation, (b): SIP (F9-HMc-FFD) simulation, (c): observation from Flight 9 between 19:55 and 21:20 UTC, and (d): the median values for each altitude for the two model simulations and observations.

Figure 9 shows the averaged values of IWC and N_i for the F9-BASE and F9-HMgc-FFD simulations between altitudes of 0.5 and 3.8 km. Comparing Figure 9a and 9c, there is a noticeable local enhancement of IWC, particularly in the western part of the simulation domain, where larger amounts of LWC and RWC are available (not shown). A similar pattern is observed for N_i (Figure 9b, d). Notably, many local enhancements in IWC and N_i are collocated with convective updrafts in the southeastern part of the domain. Despite this being a winter case, some of these updrafts reach speeds up to approximately 7 m s^{-1}, as shown in Figure 5d. Thus, convective updrafts may play a crucial role in creating favourable mixed-phase conditions for SIP (HM and FFD) even under winter conditions.

Active SIP processes not only enhance IWC and N_i but also accelerate the freezing of existing liquid water, as shown in Figure 6a and 6b. This can potentially lead to a significant reduction in the area of freezing rain near the surface. Figure 10 presents the RWC and IWC near the surface at the lowest model layer (approximately 20 m above surface) for both the F9-BASE (upper row) and F9-HMgc-FFD (lower row) simulations. The black contours indicate areas where supercooled rain is present near the surface. Comparing Figure 10a and 10c, the area of freezing rain is reduced by approximately 50% from F9-BASE to F9-HMgc-FFD case. Simultaneously, IWC in the western part of the simulation domain increases from around 0.1 g m^{-3} to 1.0 g m^{-3} from F9-BASE to F9-HMgc-FFD case.

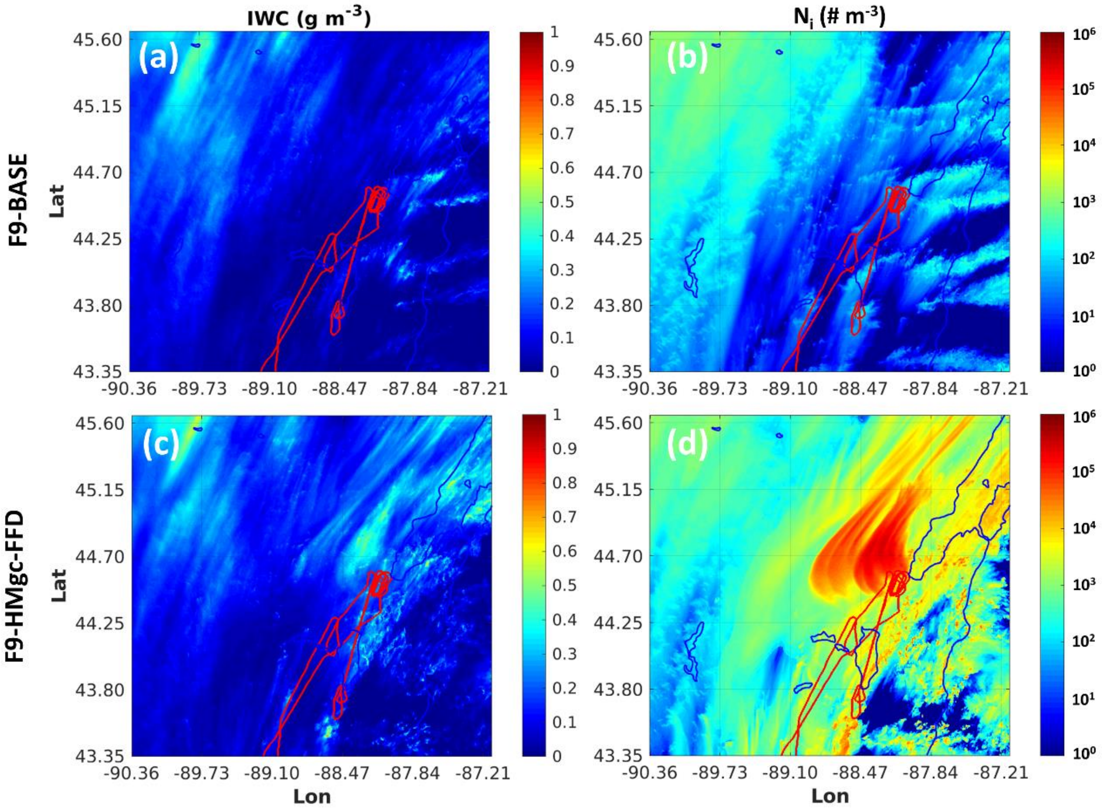

Figure 9. Averaged values between altitude of 0.5 and 3.8 km for Flight 9. (a), (c): IWC; (b), (d): Ni. Upper row for F9-BASE, lower row for F9-HMgc-FFD. Red line: flight track.

The reduction in the freezing rain area in the SIP simulation aligns more closely with observations. As shown in Figure 3, the aircraft descended to low altitudes on two occasions during missed approaches shortly before and after 20:30 UTC (indicated by yellow and turquoise arrows). During the first descent (Point 1 in Figure 3, marked by the yellow arrow), *in situ* observations indicated the presence of both IWC (Figure 3b) and LWC (Figure 3d). This descent corresponds to the yellow-highlighted flight path in Figure 10. Both simulations predict the coexistence of liquid and ice, consistent with the observations. In the second descent (Point 2 in Figure 3, marked by the turquoise arrow), high IWC values between 0.7 and 1.0 g m^{-3} were observed with no liquid water present, as shown in Figure 3. This second descent corresponds to the turquoise-highlighted flight path in Figure 10. In the F9-BASE simulation, both supercooled rain and IWC were predicted, and the IWC value is very low (<0.1 g m^{-3}). The F9-HMgc-FFD simulation, on the other hand, produced conditions with no RWC and high IWC, which closely matches the observations. The improved simulation of freezing rain conditions in this study is consistent with the findings of Cholette et al. (2024) in which the freezing rain areas are significantly reduced comparing to the simulation without SIP, despite only using the HM process in their study.

https://doi.org/10.5194/egusphere-2025-649
Preprint. Discussion started: 12 March 2025

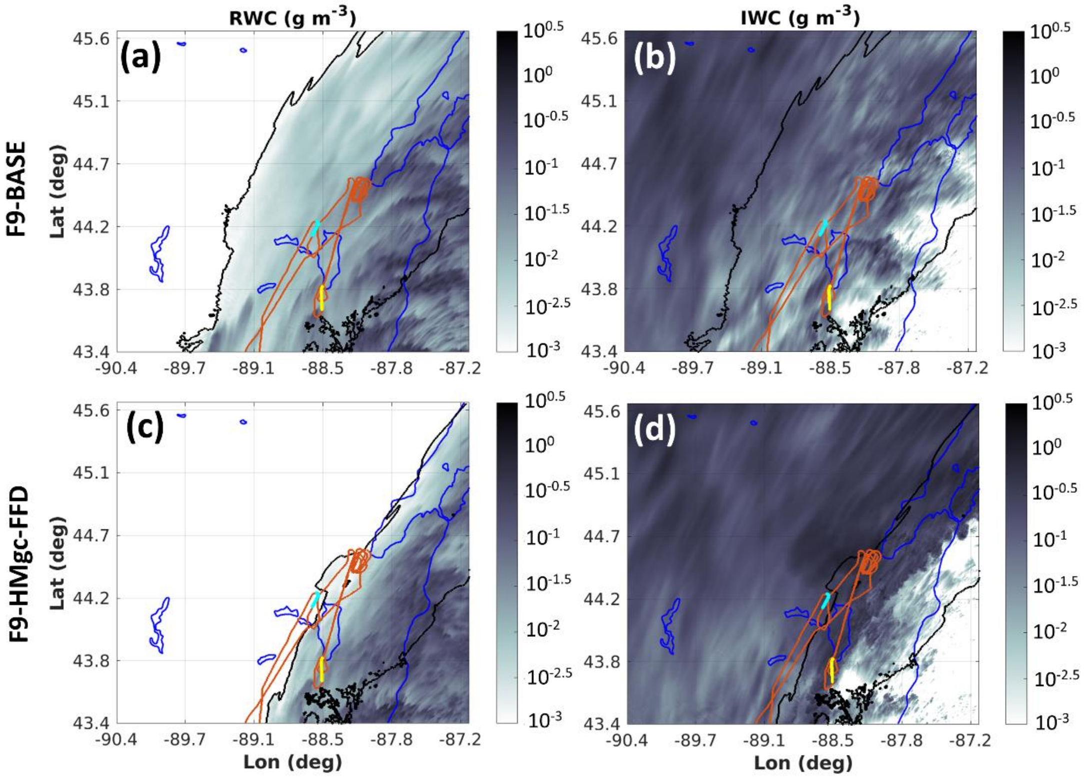

Figure 10. RWC (a, c) and IWC (b, d) near the surface for BASE (a, b) and SIP (F9-HMgc-FFD) (c, d) simulations at 20:30 UTC on 2019-02-07. Black contour: region of freezing rain (RWC > 0.01 g m^{-3} and T < 0°C in the lowest model layer at ~20 m above surface). Red lines: Flight 9 aircraft track. Yellow lines: part of flight track below 800 m of altitude observing both supercooled liquid and ice near 20:12 UTC. Turquoise lines: part of flight track below 800 m of altitude observing only ice near 20:47 UTC. 335

5.2. ICICLE Flight 20: stratiform mesoscale case

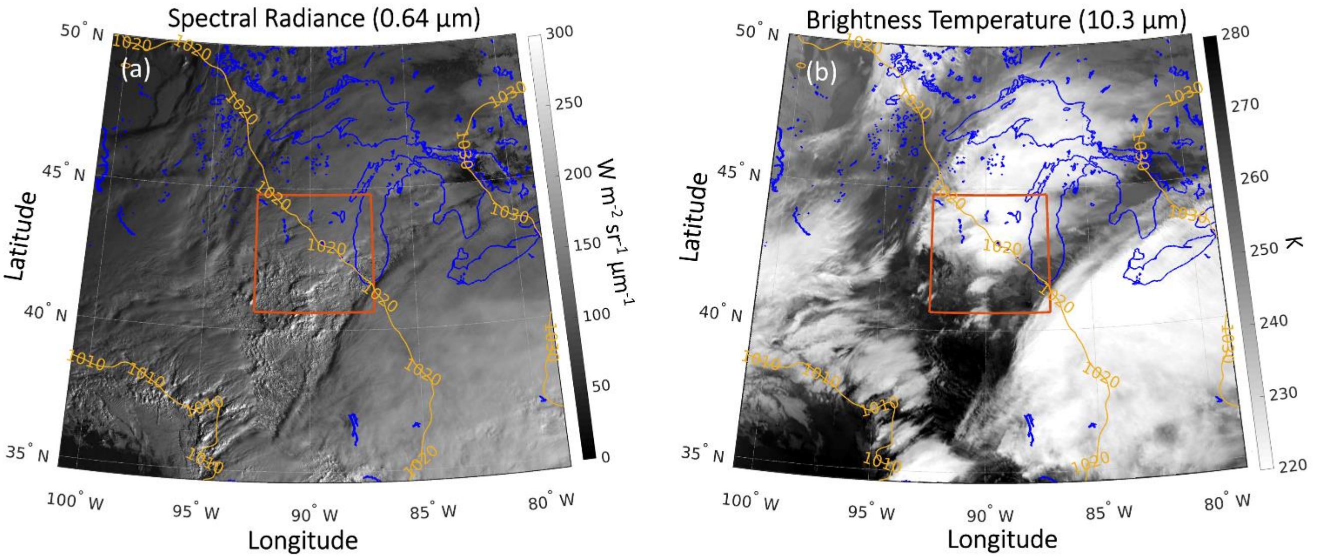

340 Figure 11. (a) GOES-16 spectral radiance at 0.64 µm (channel 2). (b) GOES-16 brightness temperature at 10.3 µm (channel 13). Both images are from 14:30 UTC on 23 February 2019. Blue lines represent coastlines, and the red rectangle represents the inner-most simulation domain at 0.25 km resolution for Flight 20.

On 23 February 2019, a significant winter storm impacted the Great Lakes region, including Wisconsin, and northern Illinois, bringing heavy snowfall, high winds, and blizzard conditions. Satellite data from GOES-16 (Figure 11) indicated widespread 345 overcast conditions, with thick clouds dominating the region. The cloud cover consisted of mostly stratiform clouds, typical of large-scale winter systems.

ICICLE Flight 20 was conducted on 23 February, in the area west of Lake Michigan. The flight encountered an extensive cloud system spanning over more than 300 km, within which HIWC conditions were frequently observed. Figure 12 presents the observed X-band radar reflectivity, *in situ* data, and flight altitude. A consistent bright band was detected throughout the 350 flight. A temperature inversion was also observed as the aircraft passed through the bright band. Below the bright band, the aircraft primarily detected liquid water, often supercooled (Figure 12e), with no ice present. Above the bright band, observations indicated mostly ice, often with IWC exceeding 0.5 g m^{-3}, and little to no liquid water, particularly between 13:45 and 16:00 UTC. One exception is between 12:25 and 13:45 UTC. As a result, mixed-phase conditions were less frequent in this case compared to the previous Flight 9.

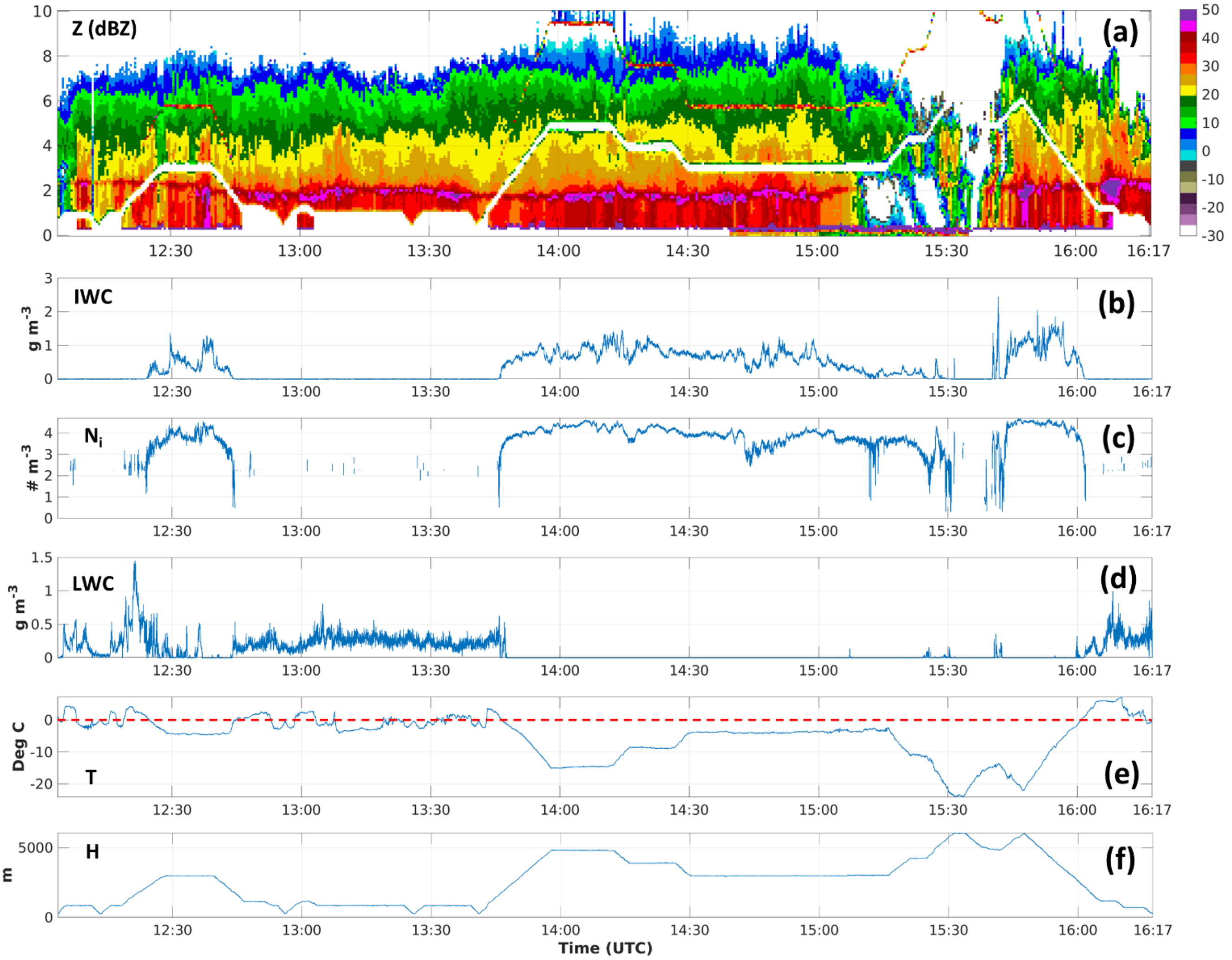

Figure 12. Same as Figure 3 but for ICICLE Flight 20 on 2019-02-23.

Figure 13 shows the simulated brightness temperature at 10.3 µm for the F20-BASE simulations (Figure 13a), along with the observed brightness temperature from GOES-16 on 23 February 2019 at 14:30 UTC (Figure 13b). The F20-BASE simulation effectively reproduces the large-scale sea-level pressure pattern (shown by yellow lines). The simulated brightness temperature at 10.3 µm closely matches the GOES-16 observations, although it slightly underestimates cloud coverage.

The simulated profiles within 10 km of the aircraft track indicate that the impact of SIP (across all three SIP simulations) on IWC and N_i is minimal (Figures 14a, c). The F20-HMgc-FFD simulation shows a maximum IWC increase of approximately 10% at 3 km altitude compared to the F20-BASE simulation. The increase in N_i is about 2-3 times, which is significantly smaller than the Flight 9 case, where increases reached 2-3 orders of magnitude. Additionally, F20-HMgc-FFD generates lower LWC and RWC above 2.5 km (Figures 15a, b). Due to the higher N_i, the Z_{median} in the F20-HMgc-FFD simulation is about 3 dBZ lower than in the F20-BASE simulation between 2 and 4 km altitude. No SIP activity is detected in any of the simulations at 14:30 UTC (Figures 15d, e) within 10 km of distance to the flight track. Note that there are regions with SIP activities at this time step, but they are away from the selected regions for statistics. The simulated case on 23 February 2019, appears more stratiform, with maximum vertical updraft velocities typically below 4 m s^{-1}. This condition likely contributes to the less frequent occurrence of mixed-phase conditions near the bright band, whereas precipitation size drops driven by updrafts through the melting layer could play a crucial role in enhancing SIP activity, as suggested by Korolev et al. (2024).

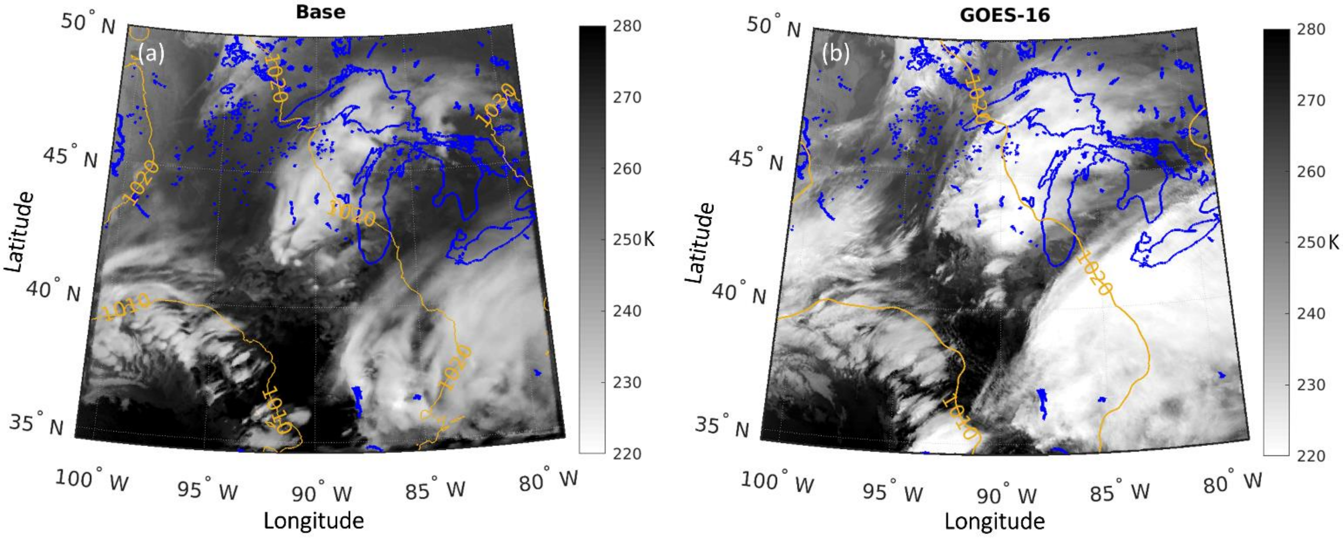

Figure 13. Similar to Figure 4 but for ICICLE Flight 20 on 23 February 2019 at 14:30 UTC. The yellow lines in panel b indicate the sea-level pressure from ECCC's operation regional prediction at 14:30 UTC initiated at 12:00 UTC.

375 Although SIP (HM and FFD) activity during ICICLE Flight 20 is minimal in the simulation, a large area of HIWC conditions is observed. Unlike localised convective cases during the ICICLE Flight 9 or tropical cases (Korolev et al., 2024), the results from ICICLE Flight 20 suggest that HIWC conditions can develop without significant contributions from SIP processes, particularly in stratiform and long-lasting cloud systems.

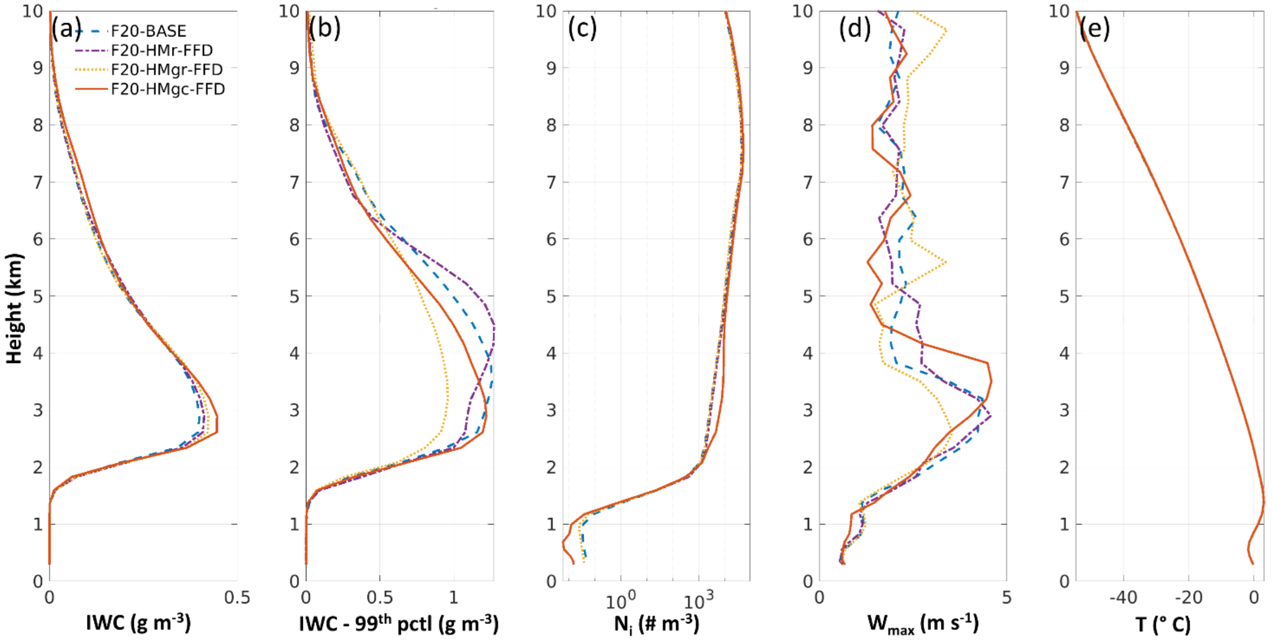

Figure 14. Same as Figure 5 but for ICICLE Flight 20 on 2019-02-23. The profiles are calculated based on simulation data at 510 min (14:30 UTC).

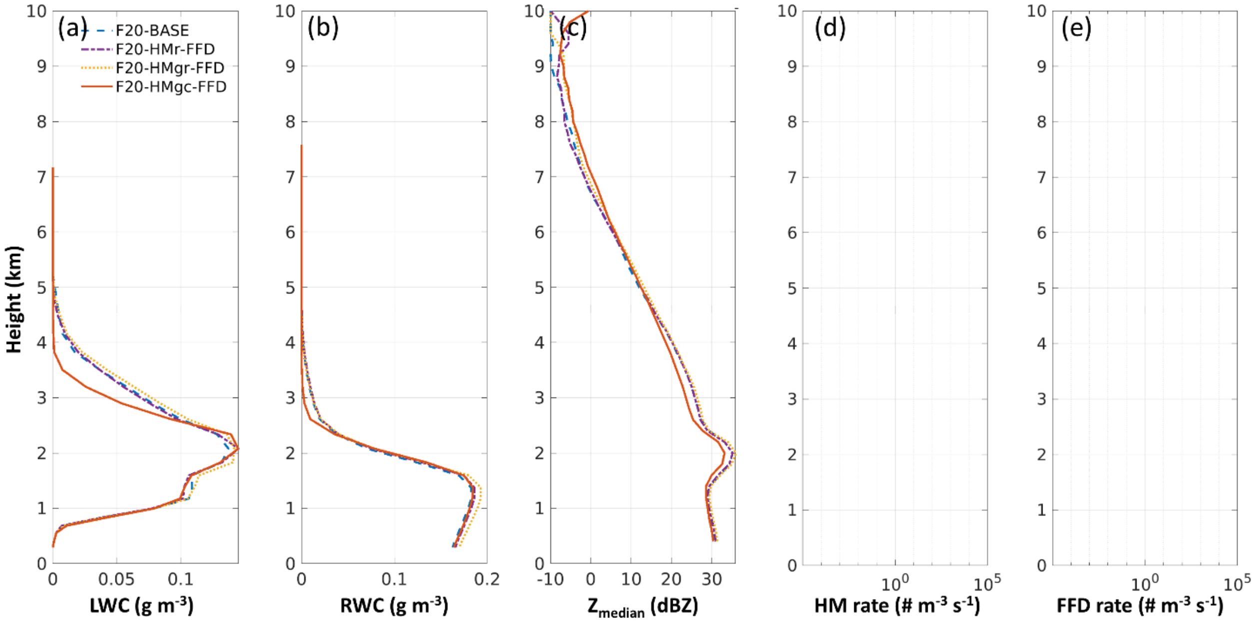

Figure 15. Same as Figure 6 but for ICICLE Flight 20 on 2019-02-23. The profiles are calculated based on simulation data at 510 min (14:30 UTC).

All simulations, including F20-BASE, show reasonably good agreement with the observations for IWC and N_i, as illustrated in Figure 16. Unlike the ICICLE Flight 9 case, the F20-BASE simulation does not significantly underestimate the frequency of HIWC conditions. For the N_i distribution, while F20-HMgc-FFD provides the closest match to the observations, the F20-BASE simulation also produces a fairly accurate estimate.

390 One possible reason for the fairly accurate N_i values in the F20-BASE simulation is that in this stratiform case N_i is primarily governed by the homogeneous freezing process, with SIP playing a relatively less important role. Ice particles with high number concentrations, formed through homogeneous freezing above 7 km, fall and eventually increase N_i values at lower altitudes. The persistence of this long-lasting cloud system, which endured for more than 6 hours at 14:30 UTC, facilitates this process.

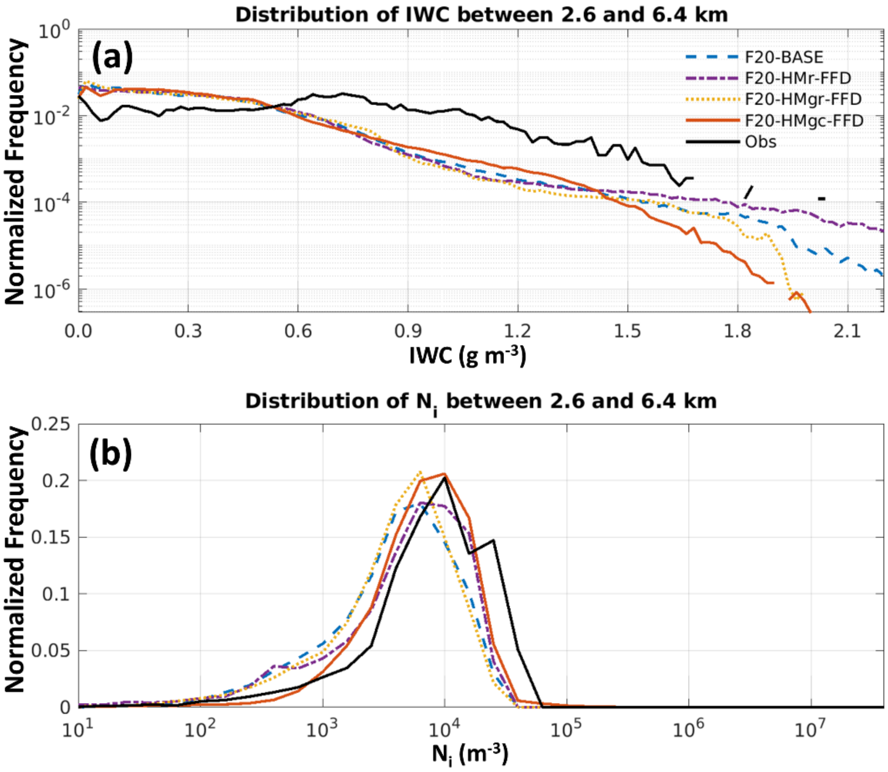

395

Figure 16. Same as Figure 7 but for simulations at 14:30 UTC on 2019-02-23 and observation data from ICICLE Flight 20. The altitude range is between 2.6 and 6.4 km.

A similar conclusion can be drawn from the 2D histogram of Z and the Z_{median} profiles shown in Figure 17. There is a good agreement in Z_{median} between the simulation and observation for both the F20-BASE and F20-HMgc-FFD simulations between 400 2 and 4 km altitude. However, both simulations underestimate Z_{median} above 4 km.

Several factors may contribute to the underestimation of Z_{median} at higher altitudes, including uncertainties in the initial conditions of the simulation and the exclusion of certain SIP processes. One additional key source of uncertainty is related to the parameterized collection efficiency amongst ice particles. Among the available parameterizations, the range varies by nearly two orders of magnitude between the highest (Lin et al., 1983) and lowest (Ferrier et al., 1995) estimates (Khain and Pinsky, 2018). The current study employs the parameterization from Cotton et al. (1986), which represents a mid-range approach.

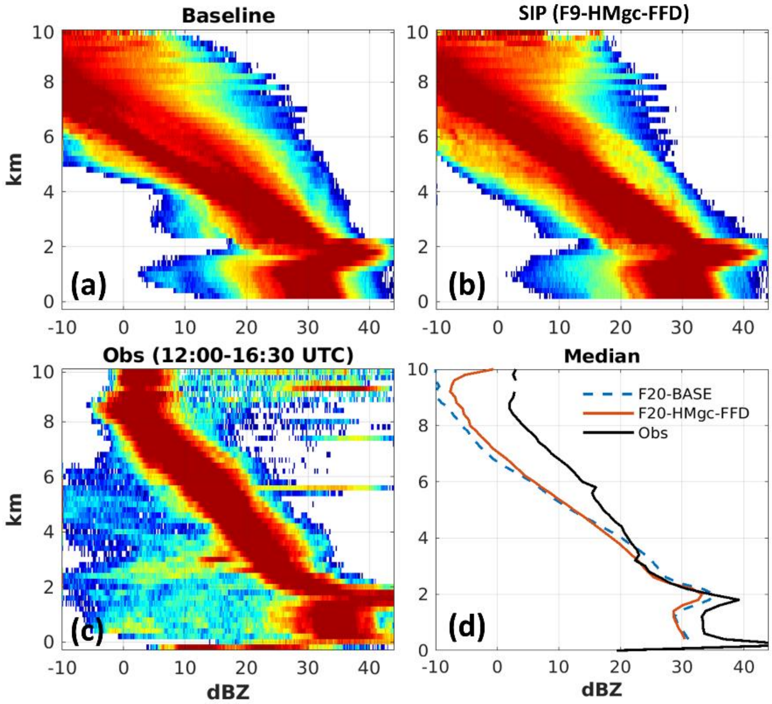

Figure 17. Similar to Figure 8 but for ICICLE Flight 20. The simulation data at 14:30 UTC on 2019-02-23 are used. The observation data from Flight 20 between 12:00 and 16:30 UTC are used.

Figure 18 shows the averaged IWC and N_i between 2.6 and 6.4 km for the F20-BASE and F20-HMgc-FFD simulations. Although the overall differences between the two simulations are relatively small, minor variations in IWC and N_i are noticeable, particularly in localized areas in the western part of the domain. These localized enhancements in IWC and N_i correspond to the locations of updrafts, albeit weaker in this case. The impact on domain-averaged IWC and N_i remains small. Although Figure 15d and 15e show no SIP activity at this specific time step within 10 km of distance to the flight track, the local enhancements of IWC and N_i in close regions to the flight track are the results of SIP processes from earlier time steps.

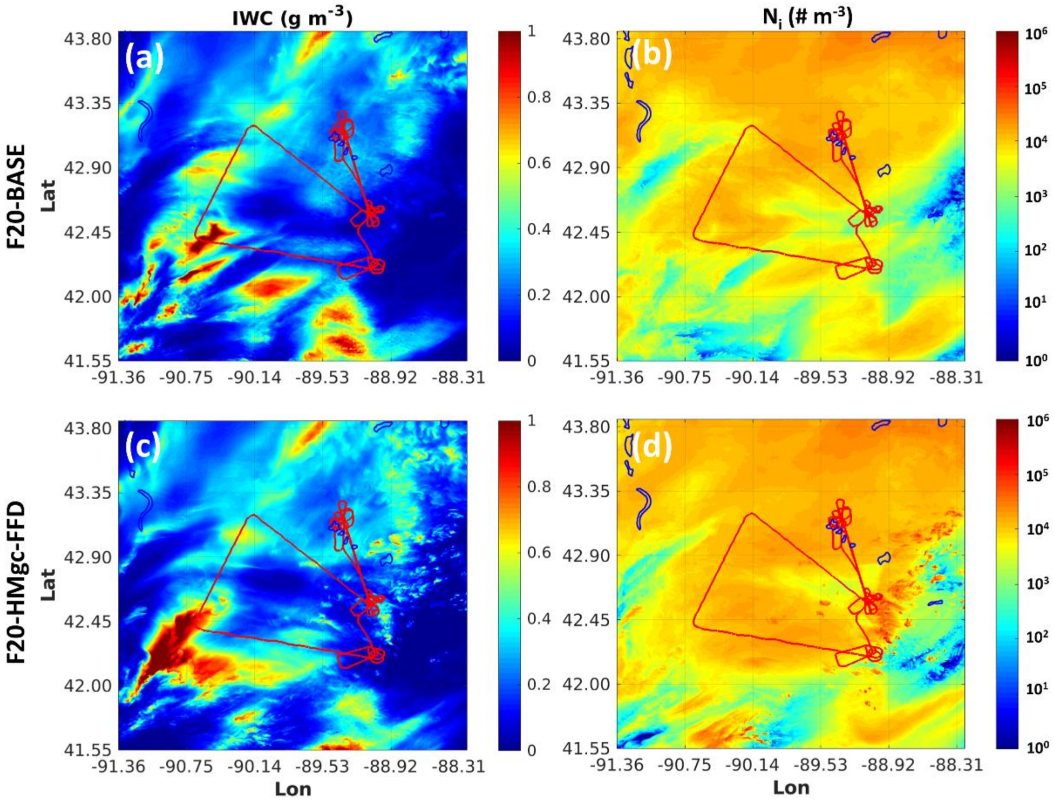

Figure 18. Similar to Figure 9 but for ICICLE Flight 20. The averaging altitudes are between 2.6 and 6.4 km. The time of the simulation is at 14:30 UTC

6. Ice particle size distribution for tropical and mid-latitude winter cases

The two mid-latitude winter cases in this study are distinct from each other and also differ from the tropical convection cases previously studied in Huang et al. (2022), Qu et al. (2022) and Korolev et al. (2024). In tropical convection, formation of secondary ice is usually associated with convective updrafts. In mid-latitude winter convective cases, such as ICICLE Flight 9, SIP processes can still significantly influence cloud ice properties, leading to enhanced IWC and N_i. In contrast, the mid-latitude winter stratiform case, like ICICLE Flight 20, exhibits very different behavior. Due to the absence of strong convective updrafts and, consequently, fewer instances of mixed-phase conditions, the impact of SIP is minimal. Nevertheless, large areas of HIWC are still observed in this case. This suggests that SIP is neither a necessary nor a sufficient condition for HIWC formation in general. However, SIP is a forcing element which contributes to the enhancement of HIWC and an increase in its longevity (Korolev et al., 2024).

https://doi.org/10.5194/egusphere-2025-649
Preprint. Discussion started: 12 March 2025

To better understand the differences among these three situations, Figure 19 shows the mass distribution of ice particles by diameter for all three cases for the temperature range between -15°C and -5°C. The solid line represents data from all Convair-580 flights during the HAIC-HIWC campaign in French Guiana (Strapp et al., 2021). Significant SIP activity was observed in these tropical cases, where most of the ice mass is concentrated around 300 µm, with a reduced fraction of large particles above 1500 µm. The ICICLE Flight 9 case (dashed line) shows a similar distribution, with peak mass centered around 400 µm, but with a higher fraction of ice particles larger than 1500 µm compared to the tropical cases. In contrast, the ICICLE Flight 20 case (dotted line) exhibits an even larger peak mass near 600 µm and a greater fraction of mass located above 800 µm. These results suggest that the ice particle mass and size distribution may be influenced by several factors, including SIP activity, the strength of convective updrafts, and the longevity of the cloud system.

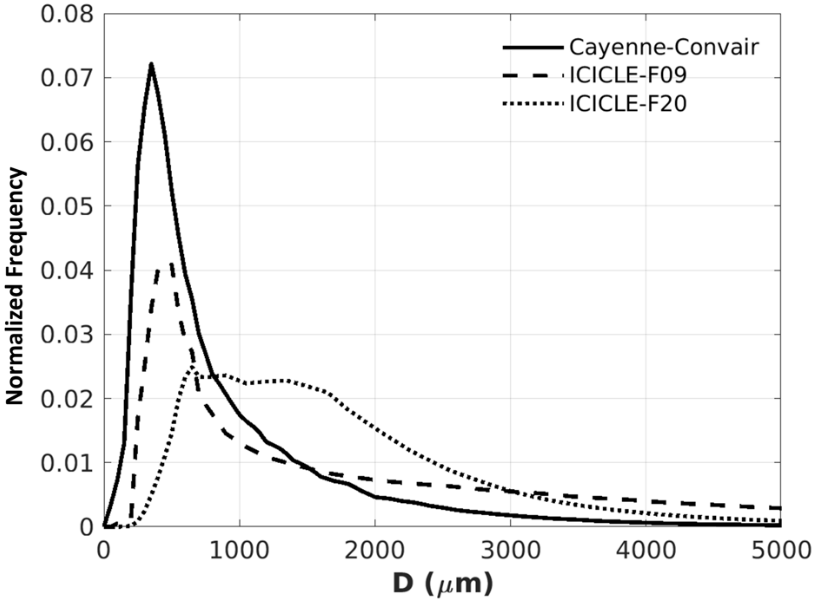

Figure 19. Observed mass distributions as a function of ice particle size (D) from Convair-580 aircraft for HAIC-HIWC campaign near French Guiana (solid line), ICICLE Flight 9 (dashed line) and ICICLE Flight 20 (dotted line) for the temperature between -15°C and -5°C.

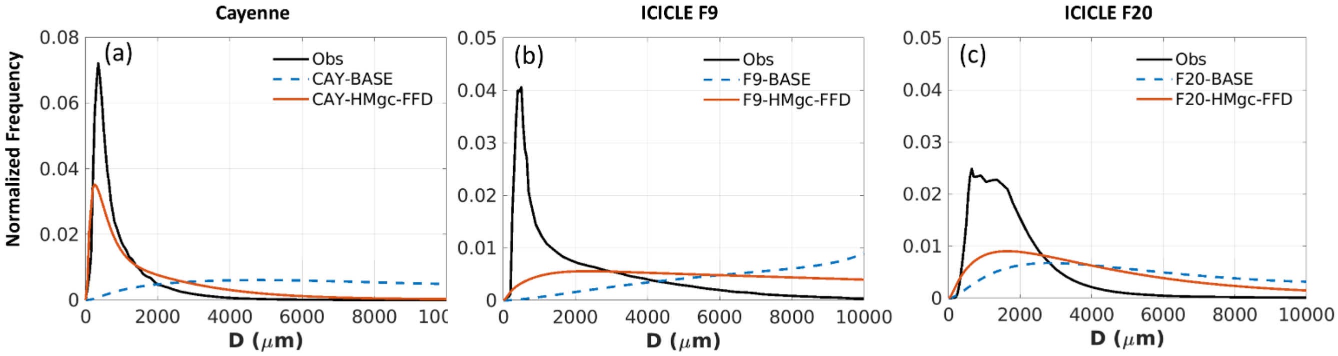

Figure 20. Ice particle mass distribution for HAIC-HIWC 2015 campaign near French Guiana (a), ICICLE Flight 9 (b), Flight 20 (c) for the temperature between -15°C and -5°C. Blue dashed lines: baseline simulation. Red lines: SIP (HMgc-FFD) simulation. Black lines: observation. 445

Although the impact of SIP processes (HM and FFD) on cloud ice properties varies significantly depending on cloud conditions, such as in ICICLE Flight 9 versus ICICLE Flight 20, incorporating these SIP processes into the P3 microphysics scheme consistently improves the representation of ice particle size distribution. This is evident for the tropical case (Figure 20a), ICICLE Flight 9 (Figure 20b), and ICICLE Flight 20 (Figure 20c). Without SIP, the BASE simulations tend to produce a larger fraction of ice with larger particle sizes. However, even with SIP, the PSD is not yet perfectly captured. Further studies are needed to enhance the accuracy of ice particle size distribution representation.

7. Conclusions and perspectives

This study examined the impact of two SIP mechanisms, HM and FFD, on two mid-latitude winter cloud cases. For the localized convective case (ICICLE Flight 9), where more vigorous updrafts are present, SIP significantly enhances IWC and N_i while reducing LWC, RWC, and Z_{median}. Activating parameterized SIP processes in the simulations results in cloud properties that compare more closely with observational data. In contrast, for the stratiform condition observed in ICICLE Flight 20, the impacts of SIP are much less pronounced, although the inclusion of SIP still provides slight improvements in the simulated cloud properties.

For localized convective cases like ICICLE Flight 9, which had a temperature inversion and freezing rain, the outcomes of SIP are highly sensitive to how different SIP mechanisms are parameterized. In particular, the ice splinters generated by HM process could trigger the FFD process. Under freezing rain conditions, where there is an abundance of supercooled raindrops, reaching a critical amount of ice particles can trigger the FFD process in a chain-reaction-like manner, leading to unrealistically high N_i values. Therefore, accurately quantifying each SIP mechanism is essential for better simulating the cloud properties. The recent laboratory study by Seidel et al. (2024), which found no strong evidence for the efficiency of the rime-splintering mechanism, which is in contrast to past studies including Hallet and Mossop, 1974, thus underscoring the need for a better understanding and more precise quantification of SIP processes.

This study also demonstrated that incorporating SIP in NWP models can significantly improve the prediction of freezing rain conditions, which is especially important in mid-latitude regions with severe winter weather. Although, in this study, the simulation results at 250 m grid spacing were primarily discussed, similar conclusions were also found for simulations at other spatial resolutions, specifically at 1 km and 2.5 km grid spacing, which are more commonly used in operational high-resolution NWP systems. Without SIP, the numerical model might overestimate the extent of freezing rain, leading to higher false alarms and unnecessary public safety concerns. Consistent findings have been reported in other studies, such as Cholette et al. (2024), which showed that including the HM process alone in a 2.5 km NWP system can notably improve freezing rain forecasts. Thus, integrating SIP processes into operational systems holds promise for enhancing the accuracy of simulated cloud and precipitation properties.

Aviation authorities recognize HIWC environment as one of the hazards for operation of commercial aviation leading to engine power loss, stalls, or damage (e.g., Lawson et al. 1998; Mason and Grzych, 2011, Brawin and Strapp 2019). Knowledge of ice particle size distributions in HIWC environment are important for aircraft engine design to mitigate their icing. The present study suggests PSDs in HIWC conditions may be significantly different compared to those observed in tropics (Strapp et al., 2021). This conclusion is also consistent with the *in situ* observations of PSDs in HIWC in Rugg et al. (2022). Altogether, this indicates the presence of regional and seasonal variations in HIWC microphysical parameters.

Finally, while simulations incorporating the activated SIP process showed improvements relative to observations, this does not imply that the current HM and FFD parameterizations accurately represent the underlying physical processes. Although these formulations draw from laboratory experiments or combined modeling and observational studies, they remain largely *ad hoc*. This research emphasizes the importance of these processes in mid-latitude winter cloud systems and highlights the need to incorporate them into numerical models. However, developing parameterizations that truly capture the detailed physics, beyond just bulk effects, remains to be topics of research.

Code and Data Availability

In situ data are available from the Earth Observation Laboratory (EOL) archive 1265 https://doi.org/10.26023/PSC2-TTQS-390A. The GEM code (version 5.1.0-rc3) is available from https://github.com/ECCC-ASTD-MRD/gem/tree/5.1.0-rc3 (Environment and Climate Change Canada, 2020). The code for the P3 microphysics scheme used is available at https://github.com/P3-microphysics/P3-microphysics (Environment and Climate Change Canada and National Center for Atmospheric Research, 2023). Configuration files to reproduce the GEM simulations are available upon request.

Authors Contribution

ZQ, AK and JM conceptualized the research goals and aims. ZQ, JM and AK designed the experiments. AK, IH, MW, CN collected and processed ICICLE data. ZQ performed the simulations and analysis with the help from AK, JM, IH, MW and CN. ZQ prepared the manuscript with contributions from all co-authors.

Competing interests

The authors declare that they have no conflict of interest.

Acknowledgement

The authors thank Manon Faucher (ECCC) for her help with setting up the GEM model.

References

Ackerman, A., Fridlind, A., Grandin, A., Dezitter, F., Weber, M., Strapp, J., and Korolev, A.: High ice water content at low radar reflectivity near deep convection–Part 2: Evaluation of microphysical pathways in updraft parcel simulations, Atmospheric Chemistry and Physics, 15, 11 729–11 751, https://doi.org/10.5194/acp-15-11729-2015, 2015.

Bernstein, B., DiVito, S., Riley, J.T., Landolt, S., Haggerty, J., Thompson, G., Adriaansen, D., Serke, D., Kessinger, C., Tessendorf, S., Wolde, M., Korolev, A., Brown, A., Nichman, L., Sims, D., Dumont, C.: The In-Cloud Icing and Large-Drop Experiment Science and Operations Plans [DOT/FAA/TC-21/29]. https://doi.org/10.21949/1524472, 2021a

Bernstein, B., DiVito, S., Riley, J., Landolt, S. D., Sims, D., Haggerty, J., Korolev, A., Heckman, I., Wolde, M., Nichman, L., Brown, A.: Overview of NRC Convair-580 *in situ* flight observations made during ICICLE. 21st Conf. on Aviation, Range, and Aerospace Meteorology, Amer. Meteor. Soc., 10.4A, https://ams.confex.com/ams/101ANNUAL/meetingapp.cgi/Paper/384109, 2021b.

Bravin, M. and Strapp, J.W.: A Continuing Investigation of Diurnal and Location Trends in an Ice Crystal Icing Engine Event Database," *SAE Int. J. Advances & Curr. Prac. in Mobility* 2(1):90-105, 2020, doi:10.4271/2019-01-1964, 2019.

Cantrell, W. and Heymsfield, A.: Production of ice in tropospheric clouds: A review, Bulletin of the American Meteorological Society, 86, 795–808, https://doi.org/10.1175/BAMS-86-6-795, 2005.

Côté, J., Gravel, S., Méthot, A., Patoine, A., Roch, M. and Staniforth, A.: The operational CMC–MRD global environmental multiscale (GEM) model. Part I: Design considerations and formulation. Monthly Weather Review, 126, 1373–1395. https://doi.org/10.1175/1520-0493(1998)126,1373:TOCMGE.2.0.CO;2, 1998.

Dedekind, Z., Lauber, A., Ferrachat, S., and Lohmann, U.: Sensitivity of precipitation formation to secondary ice production in winter orographic mixed-phase clouds, Atmos. Chem. Phys., 21, 15115–15134, https://doi.org/10.5194/acp-21-15115-2021, 2021.

DiVito, S., Bernstein, B. C., Sims, D. L., J. Riley, T., Landolt, S. D., Haggerty, J. A., Wolde, M., and Korolev, A.: In-Cloud Icing and Large-Drop Experiment (ICICLE). Part I: Overview. 20th Conf. on Aviation, Range, and Aerospace Meteorology, Boston, MA, Amer. Meteor. Soc., https://ams.confex.com/ams/2020Annual/videogateway.cgi/id/518662?recordingid=518662, 2020

Cholette, M., Milbrandt, J. A., Morrison, H., Kirk, S., and Lalonde, L.-É.: Secondary ice production improves simulations of freezing rain. Geophysical research letters, 51(8), 108490 (11 pages). https://doi.org/10.1029/2024gl108490, 2024.

Cholette, M., Milbrandt, J. A., Morrison, H., Paquin-Ricard, D., and Jacques, D.: Combining triple-moment ice with prognostic liquid fraction in the P3 microphysics scheme: Impacts on a simulated squall line. Journal of Advances in Modeling Earth Systems, 15(4), e2022MS003328. https://doi.org/10.1029/2022ms003328, 2023.

Cholette, M., Morrison, H., Milbrandt, J. A., and Thériault, J. M.: Parameterization of the bulk liquid fraction on mixed-phase particles in the Predicted Particle Properties (P3) scheme: Description and idealized simulations. Journal of the Atmospheric Sciences, 76(2), 561– 582. https://doi.org/10.1175/jas-d-18-0278.1, 2019.

Cotton, W. R., Tripoli, G. J., Rauber, R. M., & Mulvihill, E. A.: Numerical Simulation of the Effects of Varying Ice Crystal Nucleation Rates and Aggregation Processes on Orographic Snowfall. Journal of Climate and Applied Meteorology, 25(11), 1658–1680. http://www.jstor.org/stable/26183490, 1986.

Dye, J. E., and Hobbs P. V.: The influence of environmental parameters on the freezing and fragmentation of suspended water drops. J. Atmos. Sci., 25, 82–96, https://doi.org/10.1175/1520-0469(1968)025<0082:TIOEPO>2.0.CO;2, 1968.

Environment and Climate Change Canada: The Global Environmental Multiscale Model (GEM) (version 5.1.0-rc3), GitHub [code], https://github.com/ECCC-ASTD-MRD/gem/tree/5.1.0-rc3 (last access 18 October 2024), 2020.

Environment and Climate Change Canada and National Center for Atmospheric Research: Predicted Particle Properties (P3) bulk microphysics scheme, GitHub [code], https://github.com/P3-microphysics/P3-microphysics (last access 18 October 2024), 2023.

Ferrier, B. S., W.-K. Tau, and J. Simpson: A two-moment multiple phase four-class bulk ice scheme. Part II: Simulations of convective storms in different large-scale environments and comparisons with other bulk parameterizations. J. Atmos. Sci., 52, 1001–1033, 1995.

Field, P. R., Lawson, R. P., Brown, P. R. A., Lloyd, G., Westbrook, C., Moisseev, D., Miltenberger, A., Nenes, A., Blyth, A., Choularton, T., Connolly, P., Buehl, J., Crosier, J., Cui, Z., Dearden, C., DeMott, P., Flossmann, A., Heymsfield, A., Huang, Y., Kalesse, H., Kanji, Z. A., Korolev, A., Kirchgaessner, A., Lasher-Trapp, S., Leisner, T., McFarquhar, G., Phillips, V., Stith, J., and Sullivan, S.: Secondary Ice Production: Current State of the Science and Recommendations for the Future, Meteor. Mon., 58, 7.1–7.20, https://doi.org/10.1175/amsmonographs-d-16-0014.1, 2017.

Franklin, C. N., Protat, A., Leroy, D., and Fontaine, E.: Controls on phase composition and ice water content in a convection-permitting model simulation of a tropical mesoscale convective system, Atmospheric Chemistry and Physics, 16, 8767–8789, https://doi.org/10.5194/acp-445 16-8767-2016, 2016.

Fridlind, A. M., Ackerman, A. S., Grandin, A., Dezitter, F., Weber, M., Strapp, J. W., Korolev, A. V., and Williams, C. R.: High ice water content at low radar reflectivity near deep convection – Part 1: Consistency of *in situ* and remote-sensing observations with stratiform rain column simulations, Atmos. Chem. Phys., 15, 11713–11728, https://doi.org/10.5194/acp-15-11713-2015, 2015.

Fu, S., Deng, X., Shupe, M. D., and Xue, H.: A modelling study of the continuous ice formation in an autumnal Arctic mixed-phase cloud case, Atmospheric Research, 228, 77–85, https://doi.org/10.1016/j.atmosres.2019.05.021, 2019.

Gayet, J.-F., and Coauthors : On the observation of unusual high concentration of small chain-like aggregate ice crystals and large ice water contents near the top of a deep convective cloud during the CIRCLE-2 experiment, Atmos. Chemistry and Physics, 12 (2), 727-744, https://doi:10.5194/acp-12-727-2012, 2012

Girard, C., Desgagné, M., McTaggart-Cowan, R., Côté, J., Charron, M., Gravel, S., Lee, V., Patoine, A., Qaddouri, A., Roch, M., Spacek, L., Tanguay, M., Vaillancourt, P.A. and Zadra, A.: Staggered vertical discretization of the Canadian environmental multiscale (GEM) model using a coordinate of the log-hydrostatic-pressure type. Monthly Weather Review, 142, 1183–1196. https://doi.org/10.1175/MWR-D-13-00255.1, 2014.

Hallett, J. and Mossop, S.: Production of secondary ice particles during the riming process, Nature, 249, 26–28, https://doi.org/10.1038/249026a0, 1974.

Hawker, R. E., Miltenberger, A. K., Johnson, J. S., Wilkinson, J. M., Hill, A. A., Shipway, B. J., Field, P. R., Murray, B. J., and Carslaw, K. S.: Model emulation to understand the joint effects of ice-nucleating particles and secondary ice production on deep convective anvil cirrus, Atmos. Chem. Phys., 21, 17315–17343, https://doi.org/10.5194/acp-21-17315-2021, 2021.

Heymsfield, A. J., and Palmer, A.: Relationship for deriving thunderstorm anvil ice mass for CCOPE storm weather estimates, J. Clim. Appl. Meteorol., 25, 691–702, https://doi.org/10.1175/1520-0450(1986)025<0691:RFDTAI>2.0.CO;2, 1986.

Hoarau, T., Pinty, J.-P., and Barthe, 455 C.: A representation of the collisional ice break-up process in the two-moment microphysics LIMA v1.0 scheme of Meso-NH, Geoscientific Model Development, 11, 4269–4289, https://doi.org/10.5194/gmd-11-4269-2018, 2018.

Hobbs, P. V. and Rangno, A. L.: Ice particle concentrations in clouds, Journal of Atmospheric Sciences, 42, 2523–2549, https://doi.org/10.1175/1520-0469(1985)042<2523:IPCIC>2.0.CO;2, 1985.

Huang, Y., Wu, W., McFarquhar, G. M., Wang, X., Morrison, H., Ryzhkov, A., Hu, Y., Wolde, M., Nguyen, C., Schwarzenboeck, A., et al.: Microphysical processes producing high ice water contents (HIWCs) in tropical convective clouds during the HAIC-HIWC field campaign: evaluation of simulations using bulk microphysical schemes, Atmospheric Chemistry and Physics, 21, 6919–6944, https://doi.org/10.5194/acp-21-6919-2021, 2021.

Huang, Y., Wu, W., McFarquhar, G. M., Xue, M., Morrison, H., Milbrandt, J., Korolev, A. V., Hu, Y., Qu, Z., Wolde, M., Nguyen, C., Schwarzenboeck, A., and Heckman, I.: Microphysical processes producing high ice water contents (HIWCs) in tropical convective clouds during the HAIC-HIWC field campaign: dominant role of secondary ice production, Atmos. Chem. Phys., 22, 2365–2384, https://doi.org/10.5194/acp-22-2365-2022, 2022.

Khain, A. P., & Pinsky, M.: Physical processes in clouds and cloud modeling. Cambridge University Press, 2018.

Kleinheins, J., Kiselev, A., Keinert, A., Kind, M., and Leisner, T.: Thermal imaging of freezing drizzle droplets: pressure release events as a source of secondary ice particles, J. Atmos. Sci., 78, 1703–1713, https://doi.org/10.1175/jas-d-20-0323.1, 2021.

Korolev, A. and Leisner, T.: Review of experimental studies of secondary ice production, Atmospheric Chemistry and Physics, 20, 11 767–11 797, https://doi.org/10.5194/acp-20-11767-2020, 2020.

Korolev, A., Qu, Z., Milbrandt, J., Heckman, I., Cholette, M., Wolde, M., Nguyen, C., McFarquhar, G., Lawson, P., and Fridlind, A.: High ice water content in tropical mesoscale convective systems (a conceptual model), EGUsphere [preprint], https://doi.org/10.5194/egusphere-2024-1465, 2024.

Lachapelle, M., Cholette, M., and Thériault, J. M.: Effect of Secondary Ice Production Processes on the Simulation of ice pellets using the Predicted Particle Properties microphysics scheme, EGUsphere [preprint], https://doi.org/10.5194/egusphere-2024-594, 2024.

Ladino, L. A., Korolev, A., Heckman, I., Wolde, M., Fridlind, A. M., and Ackerman, A. S.: On the role of ice-nucleating aerosol in the formation of ice particles in tropical mesoscale convective systems, Geophysical research letters, 44, 1574–1582, https://doi.org/10.1002/2016GL072455, 2017.

Lawson, R. P., Angus, L. J., and Heymsfield, A. J., Cloud Particle Measurements in Thunderstorm Anvils and Possible Threat to Aviation, Journal of Aircraft, 35, 1, 1998, 113–121, 1998.

Lawson, R. P., Woods, S., and Morrison, H.: The microphysics of ice and precipitation development in tropical cumulus clouds, J. Atmos. Sci., 72, 2429–2445, https://doi.org/10.1175/JAS-D-14-0274.1, 2015

Leroy, D., Fontaine, E., Schwarzenboeck, A., Strapp, J.W., Korolev, A., McFarquhar, G., Dupuy, R., Gourbeyre, C., Lilie, L., Protat, A., et al.: Ice crystal sizes in high ice water content clouds. Part II: Statistics of mass diameter percentiles in tropical convection observed during the HAIC/HIWC project, Journal of Atmospheric and Oceanic Technology, 34, 117–136, https://doi.org/10.1175/JTECH-D-15-0246.1, 2017.

Lin, Y.-L., Farley, R. D., & Orville, H. D.: Bulk parameterization of the snow field in a cloud model. Journal of Climate and Applied Meteorology, 22, 1065– 1092. https://doi.org/10.1175/1520-0450(1983)022<1065:bpotsf>2.0.co;2, 1983.

Mason, J.G., Strapp, J.W., and Chow, P., The Ice Particle Threat to Engines in Flight, 44th AIAA Aerospace Sciences Meeting and Exhibit, Reno, Nevada, January 9–12, 2006.

Mason, J.G., and Grzych, M., “The Challenges Identifying Weather Associated with Jet Engine Ice Crystal Icing,” SAE Technical Paper 2011-38-0094, https://doi.org/10.4271/2011-38-0094, 2011.

Milbrandt, J. A., Morrison, H., Dawson, D. T., II, and Paukert, M.: A triple-moment representation of ice in the Predicted Particle Properties (P3) microphysics scheme. J. Atmos. Sci., 78, 439– 458. https://doi.org/10.1175/JAS-D-20-0084.1, 2021.

Milbrandt, J. A. and Morrison, H.: Parameterization of cloud microphysics based on the prediction of bulk ice particle properties. Part III: Introduction of multiple free categories, J. Atmos. Sci., 73, 975–995, https://doi.org/10.1175/JAS-D-15-0204.1, 2016.

Morrison, H. and Milbrandt, J. A.: Parameterization of cloud microphysics based on the prediction of bulk ice particle properties. Part I: Scheme description and idealized tests, J. Atmos. Sci., 72, 287–311, https://doi.org/10.1175/JAS-D-14-0065.1, 2015.

Morrison, H. and Milbrandt, J. A. and Cholette, M.: A complete triple-moment representation of ice in the Predicted Particle Properties (P3) microphysics scheme. *J.A.M.E.S* (under review).

Oraltay, R. G. and Hallett, J.: Evaporation and melting of ice crystals: A laboratory study, Atmos. Res., 24, 169–189, https://doi.org/10.1016/0169-8095(89)90044-6, 1989.

Phillips, V. T., Yano, J.-I., Formenton, M., Ilotoviz, E., Kanawade, V., Kudzotsa, I., Sun, J., Bansemer, A., Detwiler, A. G., Khain, A., et al.: Ice multiplication by breakup in ice–ice collisions. Part II: Numerical simulations, Journal of the Atmospheric Sciences, 74, 2789–2811, https://doi.org/10.1175/JAS-D-16-0223.1, 2017.

Phillips, V. T., Patade, S., Gutierrez, J., and Bansemer, A.: Secondary ice production by fragmentation of freezing drops: Formulation and theory, Journal of the Atmospheric Sciences, 75, 3031–3070, https://doi.org/10.1175/JAS-D-17-0190.1, 2018.

Prabhakaran, P., Kinney, G., Cantrell, W., Shaw, R. A., & Bodenschatz, E.: High supersaturation in the wake of fallinghydrometeors: Implications for cloud invigoration and ice nucleation.Geophysical Research Letters,47, e2020GL088055. https://doi.org/10.1029/2020GL088055, 2020.

James, R. L., Phillips, V. T. J., and Connolly, P. J.: Secondary ice production during the break-up of freezing water drops on impact with ice particles, Atmos. Chem. Phys., 21, 18519–18530, https://doi.org/10.5194/acp-21-18519-2021, 2021.

Qu, Z., Barker, H. W., Korolev, A. V., Milbrandt, J. A., Heckman, I., Bélair, S., Leroyer, S., Vaillancourt, P. A., Wolde, M., Schwarzenböck, A., et al.: Evaluation of a high-resolution numerical weather prediction model's simulated clouds using observations from CloudSat, GOES-13 and *in situ* aircraft, Quarterly Journal of the Royal Meteorological Society, 144, 1681–1694, https://doi.org/10.1002/qj.3318, 2018.

Qu, Z., Korolev, A., Milbrandt, J. A., Heckman, I., Huang, Y., McFarquhar, G. M., Morrison, H., Wolde, M., and Nguyen, C.: The impacts of secondary ice production on microphysics and dynamics in tropical convection, EGUsphere [preprint], https://doi.org/10.5194/egusphere-2022-235, 2022.

Rugg, A.; Bernstein, B.C.; Haggerty, J.A.; Korolev, A.; Nguyen, C.; Wolde, M.; Heckman, I.; DiVito, S. High Ice Water Content Conditions Associated with Wintertime Elevated Convection in the Midwest. *J. Appl. Meteorol. Climatol.* 2022, *61*, 559–575, https://doi.org/10.1175/JAMC-D-21-0189.1, 2022

Saunders, R., Hocking, J., Turner, E., Rayer, P., Rundle, D., Brunel, P., Vidot, J., Roquet, P., Matricardi, M., Geer, A., Bormann, N., and Lupu, C.: An update on the RTTOV fast radiative transfer model (currently at version 12), Geosci. Model Dev., 11, 2717–2737, https://doi.org/10.5194/gmd-11-2717-2018, 2018.

Seidel, J. S., Kiselev, A. A., Keinert, A., Stratmann, F., Leisner, T., and Hartmann, S.: Secondary ice production – no evidence of efficient rime-splintering mechanism, Atmos. Chem. Phys., 24, 5247–5263, https://doi.org/10.5194/acp-24-5247-2024, 2024.

Sotiropoulou, G., Sullivan, S., Savre, J., Lloyd, G., Lachlan-Cope, T., Ekman, A. M., and Nenes, A.: The impact of secondary ice production on Arctic stratocumulus, Atmospheric Chemistry and Physics, 20, 1301–1316, https://doi.org/10.5194/acp-20-1301-2020, 2020.

Sotiropoulou, G., Vignon, É., Young, G., Morrison, H., O'Shea, S. J., Lachlan-Cope, T., Berne, A., and Nenes, A.: Secondary ice production in summer clouds over the Antarctic coast: an underappreciated process in atmospheric models, Atmospheric Chemistry and Physics, 21, 755–771, https://doi.org/10.5194/acp-21-755-2021, 2021.

Stanford, M. W., Varble, A., Zipser, E., Strapp, J. W., Leroy, D., Schwarzenboeck, A., Potts, R., and Protat, A.: A ubiquitous ice size bias in simulations of tropical deep convection, Atmospheric Chemistry and Physics, 17, 9599–9621, https://doi.org/10.5194/acp-17-9599-2017, 2017.

Strapp, J. W., Schwarzenboeck, A., Bedka, K., Bond, T., Calmels, A., Delanoe, J., Dezitter, F., Grzych, M., Harrah, S., Korolev, A., Leroy, D., Lilie, L., Mason, J., Potts, R., Protat, A., Ratvasky, T., Riley, J. T., andWolde, M.: Comparisons of Cloud *In Situ* Microphysical Properties of Deep Convective Clouds to Appendix D/P Using Data from the High-Altitude Ice Crystals-High Ice Water Content and High Ice Water Content-RADAR I Flight Campaigns, SAE International Journal of Aerospace, 14, 127–159, https://doi.org/10.4271/01-14-02-0007, 2021.

Sullivan, S. C., Hoose, C., Kiselev, A., Leisner, T., and Nenes, A.: Initiation of secondary ice production in clouds, Atmospheric Chemistry and Physics, 18, 1593–1610, https://doi.org/10.5194/acp-18-1593-2018, 2018.

Takahashi, T., Nagao, Y., and Kushiyama, Y.: Possible high ice particle production during graupel–graupel collisions, J. Atmos. Sci., 52, 4523–4527, https://doi.org/10.1175/1520-0469(1995)052<4523:PHIPPD>2.0.CO;2, 1995.

Vardiman, L.: The generation of secondary ice particles in clouds by crystal–crystal collision, J. Atmos. Sci., 35, 2168–2180, https://doi.org/10.1175/1520-0469(1978)035<2168:TGOSIP>2.0.CO;2, 1978.

Wolde, M. and Pazmany, A.: NRC dual-frequency airborne radar for atmospheric research, in: 32nd Int. Conf. on Radar Meteorology, Albuquerque, NM, 22–29 October 2005, Amer. Meteor. Soc., P1R.9, available at: https://ams.confex.com/ams/32Rad11Meso/techprogram/paper_96918.htm (last access: 27 January 2020), 2005.